Journal of Molecular Structure 1328 (2025) 141299

Contents lists available at ScienceDirect

Journal of Molecular Structure

journal homepage: www.elsevier.com/locate/molstr

Ultrasound-assisted synthesis of β-cyclodextrin/hydroxyapatite composites as a green and safe additive for enhancing leather properties

Ilaria Quaratesi [a,b,*], Ioan Călinescu [c], Petre Chipurici [c], Elisa-Gabriela Dumbravă [c,d], Andrei Cucos [e], Mohamed Yassine Zaki [f], Pellegrino La Manna [g], Adrian Bercea [d], Miruna Silvia Stan [h], Stefan Michalik [i], Chloe Pearce [j], Marianne Odlyha [j], Genoveva Burca [i,k,l], Elena Badea [a,m,*]

[a] The National Research and Development Institute for Textile and Leather (INCDTP), Research branch Institute for Leather and Footwear (ICPI), Ion Minulescu Str. 93, 031215 Bucharest, Romania
[b] Alma Mater Studiorum – University of Bologna, CHIMIND, Viale Risorgimento 4, 40136 Bologna, Italy
[c] The National University of Science and Technology POLITECHNICA Bucharest, Faculty of Chemical Engineering and Biotechnology, Department of Bioresources and Polymer Science, 313 Splaiul Indipendentei 060042, Bucharest, Romania
[d] The National Institute for Laser, Plasma & Radiation Physics (INFLPR), Strada Atomistilor 409, 077125, Măgurele, Romania
[e] The National Institute for Research and Development in Electrical Engineering ICPE-CA Bucharest, Splaiul Unirii 313, 030138, Bucharest, Romania
[f] Laboratory of Complex Heterostructures and Multifunctional Materials, National institute of Materials Physics, Strada Atomiștilor 405A, 077125, Măgurele, Romania
[g] Water Science and technology group (WaSTe), Department of Civil Engineering, University of Salerno, Via Giovanni Paolo II 132, 84084, Fisciano (SA), Italy
[h] University of Bucharest, Biochemistry and Molecular Biology Department, Bulevardul Mihail Kogălniceanu 36-46, Bucharest, Romania
[i] Diamond Light Source Ltd, Didcot, OX11 0DE, UK
[j] School of Natural Sciences, Birkbeck, University of London, Malet St.,London, WC1E 7HX UK
[k] STFC, Rutherford Appleton Laboratory, Didcot, OX11 0QX, UK
[l] Faculty of Science and Engineering, The University of Manchester, Alan Turing Building, Oxford Road, Manchester, M13 9PL, UK
[m] Department of Chemistry, Faculty of Sciences, University of Craiova, Calea Bucuresti Str. 107 I, 200512 Cra-iova, Romania

ARTICLE INFO

Keywords:
-cyclodextrin
Hydroxyapatite
Composites
Ultrasound assisted synthesis
Leather tanning
Eco-efficiency

ABSTRACT

This study presents an ultrasound-assisted synthesis of β-cyclodextrin/hydroxyapatite composites to be used as green and safe auxiliaries in the tanning process. A combination of spectroscopic and non-spectroscopic techniques such as DLS (dynamic light scattering), ZP (zeta potential), XRD (X-ray diffraction), SEM (scanning electron microscopy) and ATR-FTIR (attenuated total reflectance-Fourier transform infrared spectroscopy) were used to thoroughly characterize the eight composites obtained by varying the ultrasound process parameters. While not cytotoxic, all composites had strong antibacterial action against *Brevibacterium lines, Staphylococcus aureus, Escherichia coli*, and *Staphylococcus epidermis*. All composites underwent lab-scale tanning tests, but only those exhibiting the most suitable set of tanning abilities underwent pilot-scale testing. The composites' interaction with the collagen matrix was assessed by micro-DSC (micro-differential scanning calorimetry), TG/DTG/DTA (thermal analysis), ^{1}H unilateral NMR (proton nuclear magnetic resonance), ATR-FTIR, *in-situ* temperature synchrotron-based XRD and standard tests (UNI EN ISO 3380: 2015, UNI EN ISO 2589: 2016, UNI EN ISO 105-B02:2014). Thermal stability, dye penetration, thickness, colour fastness, surface appearance and microbiological protection were all improved for the leather treated with a small amount of composite added to the wet finish float. These findings demonstrate the benefits of β-cyclodextrin/hydroxyapatite composites as safe and sustainable tanning additives.

1. Introduction

Since several decades, tannery sector has been called to face the challenge of the environmental sustainability [1–5]. According to the 2020 Social & Environmental Report (SER) of the European Leather Industry, tanning industries are still at the top of the most

* Corresponding authors.
E-mail addresses: ilaria.quaratesi2@unibo.it (I. Quaratesi), elena.badea@edu.ucv.ro (E. Badea).

https://doi.org/10.1016/j.molstruc.2024.141299
Received 15 November 2024; Received in revised form 18 December 2024; Accepted 31 December 2024
Available online 31 December 2024

environmentally impacting activities due to the processes and the hazardous chemicals involved in the supply and production chain from raw hides to finished leather [6]. The tanning process releases hazardous chemicals and wastewater, which makes it very polluting. In 2018, in response to the urgent need for environmentally friendly and sustainable manufacturing, the Union of Leather Technologists and Chemists Societies (IULTCS) [7] advocated a substantial reduction in the use of harmful chemicals routinely used in the area [8]. For instance, aldehyde-based tannins [9] and chromium salts [10,11] were shown to cause cancer, whilst bisphenol S-based polymers [12] showed a detrimental impact on the endocrine system. Greener and safer alternatives are currently being developed as a result of the demand for new tanning agents and additives that guarantee high performance of the finished product (such as antimicrobial activity, fullness, dye penetration, colour fastness, comfortability, smooth surface, flame retardancy, etc.) while avoiding potential risks to human health and the environment [13,14].

Recently, hydroxyapatite (HAp) [15], a naturally occurring mineral form of calcium apatite with the formula $Ca_{10}(OH)_2(PO_4)_6$, has been proposed as a promising eco-friendly fire-proof agent in the leather industry [16–19]. Moreover, its high-biocompatibility [20,21] and moderate antimicrobial activity [22] ensure that it poses a negligible danger to human health when added to leather. Other studies has documented various uses of HAp-based nanoparticles that can be readily manufactured and are used to replace harsh chemicals while simultaneously improving the quality of leather [23,24]. A drawback in the use of HAp, however, is its propensity to form agglomerates [25] and block the pores of the hide (the average hide's pore diameter is anout 10 μm) [26]. Avoiding these agglomerates forces the use of chemical dispersants like polyethylene glycole (PEG) or polyethylene imine (PEI) with an increase in production price. Accessibility to hides pores is critical for breathability [27], durability and comfortability [28] of leather. On top of that, it should be remembered that the diffusion of dyes and finish agents through the hides pores plays a key role in leather processing [29]. It has been found that using β-cyclodextrins (β-CDs) in hydroxyapatite conventional synthesis may help regulate the size of HAp particles [30,31]. CDs are cyclic oligomers of d-(+)-glucopyranose units (six for β-CDs) linked through α−1,4-glycoside bonding and are generally obtained by the enzymatic degradation of starch, being thus a renewable resource, relatively cheap, biodegradable and produced on an industrial scale [32,33]. They are water-soluble and able to form host-guest complexes with hydrophobic molecules, including dyes [34] and fragrance agents [35,36]. In addition, CDs have been explored as an auxiliary for the tanning process [37–39] since they can help the target molecule permeate better into the hide structure [40]. It has also been shown that CDs and HAp combination exhibits antifungal and antibacterial activity against gram-positive and gram-negative bacteria [41]. Nevertheless, examples of β-CD/HAp composites applications in leather are not yet reported in the literature. All of this information led us to assume that we could employ ultrasound (US) technology to obtain a β-CD/HAp composite that would work effectively as green additive in the tanning process.

Use of ultrasounds (US) is a novel green and promising technology for promoting interactions among various molecules and biomolecules. [42–44]. This technology offers process related and environmental advantages, including minimizing the use of hazardous chemicals and solvents, energy-saving, lower costs and easy workups [45–47]. To the best of our knowledge, no previous studies were performed to synthesize β-CD/HAp composite using the US technology.

In this study, β-CD/HAp composites were synthesised using different US equipment and varying the following process parameters: β-CD/HAp ratio, US amplitude and treatment time. The relationship between the ultrasound parameters, β-CD/HAp ratio and properties of the resulting composites were studied by DLS (dynamic light scattering), ZP (zeta potential, XRD (X-ray diffraction), SEM (scanning electron microscopy) and ATR-FTIR (attenuated total reflectance - Fourier transform infrared spectroscopy). To confirm the safety of the composites, cytotoxicity tests were conducted and their antibacterial activity assessed.

The composites' interaction with the collagen matrix was assessed by micro-DSC (micro-differential scanning calorimetry), TG/DTG (Thermogravimetry), ^{1}H unilateral NMR (proton nuclear magnetic resonance), ATR-FTIR, in-situ temperature synchrotron-based XRD and standard tests (UNI EN ISO 3380: 2015, UNI EN ISO 2589: 2016, UNI EN ISO 105- B02:2014). The most promising composite was added as a performance additive in the wet finishing float in a pilot scale test. A concentration similar to the concentration of the commercial synthetic re-tanning agents was used. Its effect on leather technical performance was tested using both conventional spectroscopic and non-spectroscopic methods (TG/DTG, ATR-FTIR, SEM and ^{1}H unilateral NMR), and standard tests (UNI EN ISO 3380: 2015, UNI EN ISO 2589: 2016, UNI EN ISO 105- B02:2014). In addition, *in-situ* temperature synchrotron-based diffraction measurements were performed to evaluate the collagen-composite matrix thermal denaturation.

2. Results and discussion

Ultrasounds are known to facilitate physical and chemical processes through several mechanisms [48,49]. Parameters like US amplitude, frequency and treatment time can be adjusted to tailor the properties of the resulting products. β-CD/HAp eco-composites were obtained via US-assisted processing, as reported in materials and methods section, the process parameters applied for each eco-additive (ED) being listed in Table 1.

2.1. Characterization of β-CD/HAp composites

2.1.1. Composites' (hydrodynamic) size and surface charge

Average composite size was determined through dynamic light scattering (DLS) analyses, and stability of the samples was investigated through measuring their zeta potentials. Size distribution and zeta potential based on dynamic light scattering (DLS) became routine methods for characterization of charged nanoparticles prior to any applications of some charged colloids. Given that the morphology of collagen 3D matrix in hide (determined by the fibers' arrangement, density, and wave angle) is non-homogeneous, with pores that can range from micropores (diameter < 2 nm) and mesopores (2 nm $<$ diameter $<$ 50 nm) to macropores (diameter > 50 nm) according to the classification of pore size made by International Union of Pure and Applied Chemistry (IUPAC), the dimension of the composites and their stability in suspension are critical for ensuring their permeation in the hide structure [24,50]. The composites' average size and size distribution in water suspension, as well as their zeta potential (ZP) were determined by DLS (dynamic light scattering) technique. The results are reported in Table 2 and Figure S1.

The impact of the US treatment duration was examined in the experiments that resulted in ED1, ED2, and ED3 composites. The total treatment time increase from 30 to 60 min caused a reduction in the particles' average size from about 700 nm to about 400 nm, and a more homogeneous polydispersity curve. A further increase of treatment time to 90 min determined a steep decrease of particles average size (37 nm), accompanied by a significant increase of polydispersity. Furthermore, ED3 nanoparticles are extremely unstable since the ZP value is in the range of ± (0–10) mV [51,52].

ED2 and ED8 composites results to be best in terms of average stability, with average dimensions able to penetrate the macropores of collagen matrix. It should be mentioned that ZP values were obtained as average values. A further examination of the ZP curves in Figure S1 reveals that all composites exhibit polydisperse behaviour [53].

US amplitude is another process parameter affecting the final size and stability of the composites. Another two experiments were performed applying a higher (50 %) and a lower (20 %) amplitude for 60 min, resulting in ED4 and ED5 composites, respectively. One would have been expected a decrease in the average size by increasing this parameter. However, the average size of ED4 composite increased to about 640

Table 1
List of the β-CD/HAp eco-composites obtained by US-assisted processing with their symbols and process parameters.

Composite symbol[a]	β-CD (g)	HAp suspension (g)	Energy (J)	Time[b] (min)	Amplitude (%)	Ratio β-CD:HAp
ED1	4	36	20,235	30	35	1:1
ED2	4	36	11,068	60	35	1:1
ED3	4	36	32,073	90	35	1:1
ED4	4	36	104,774	60	50	1:1
ED5	4	36	40,162	60	20	1:1
ED6	4	36	40,052	60	35	2:1
ED7	8	36	40,154	60	35	3:1
ED8	12	36	39,920	60	35	0.5:1

[a] Experimental setup: 20 KHz frequency; $T = 15$ °C.
[b] On-off times: 10 s on and 10 s off.

Table 2
Average size, polydispersity index (PI) and zeta potential (ZP) of the composite particles compared to those of HAp and β-CD.

Sample	ZP (mV)	Average size (nm)	PI
HAp	−23.8	2384	0.786
β-CD	−7.99	178.2	0.481
ED1	−14.8	716.7	0.468
ED2	−19.7	407.6	0.402
ED3	−1.26	36.82	0.781
ED4	−29.6	641.9	0.572
ED5	−24.2	445.2	0.478
ED6	Impossible to detect	207.9	0.426
ED7	Impossible to detect	420.0	0.346
ED8	−25.4	413.9	0.523

nm, that is 50 % more compared to ED2. This behaviour can be explained by the competition between the sonocrystallisation and fragmentation/deagglomeration processes during US processing. Presumably, by increasing the US amplitude, the aggregation prevails over fragmentation and deagglomeration [53]; this is also apparent from the ZP distribution of ED4, with a PI of 0.57. By reducing the amplitude to 20 % (ED5), the results are close to those obtained at 35 % amplitude (ED2), with a small difference in terms of the polydispersity, which seems better for ED2.

The effect of the β-CD/HAp ratio was also tested and resulted to be interesting, too. When β-CD is in moderate excess, as for ED6, the average particle size tends to decrease (Table 2 and Figure S1). Neither a larger excess of β-CD (ED7) nor an excess of HAp (ED8) has significant effect on the particles dimension. The ZP values of ED6 and ED7 suspensions could not be measured. Actually, it was found that the ZP values of high polydisperse suspensions of nanoparticle aggregates or agglomerates were not reproducible across laboratories, which highlights the need for improved surface charge test procedures and the identification of variability's causes. Ultrasonication was observed to further increase this variability [54]. Additionally, it should be mentioned that hide has a 3D porous network, hence the physical, mechanical, and organoleptic properties of leather are influenced by the tanning agents that fill the hide's pores and interact with collagen. Notably, the majority of hide's pores fall into the macropore region, which the composites developed in this work may readily fill.

2.1.2. Chemical structure, crystallinity and surface morphology of the β-CD/HAp composites

The formation and structure of β-CD/HAp composites were investigated by ATR-FTIR spectroscopy and XRD. ATR-FTIR provides information related to the presence or absence of specific functional groups, as well as the chemical structure of materials. Shifts in the frequency of absorption bands and changes in relative band intensities indicate changes in the chemical structure of the analysed sample. In our case, the ATR-FTIR absorption bands suggestive of the presence of HAp were identified in all the composites (Table S1): the absorption bands observed at 1450, 1420 and 874 cm^{-1}, indicative of the presence of carbonate anion, and vibrational bands of phosphate anion at 1024, 961, 607, 560 and 470 cm^{-1} [18,55] are present in all composites' spectra (Fig. 1).

The characteristic bands of β-CD, namely the hydroxyl groups at 3270 cm^{-1}, the vibrational band of the C—H bond at 2921 cm^{-1} and those of the C—O bond, visible at 1150, 1001, 525 cm^{-1}, including the stretching vibrations of glucopyranose, visible at 939, 858 and 755 cm^{-1}, plus the anomeric band vibration band at 856 cm^{-1} [56], were also detected in the spectra of all composites. Therefore, the presence of both the precursors has been demonstrated for all composites. Moreover, the wavenumber associated to the stretching of O—H bond exhibits a decrease in β-CD/HAp composite, most likely due to hydrogen bonding between OH group of β-CD and Ca^{2+} ions of HAp. It is worth noting that the characteristic band of -CH_2- in β-CD, corresponding to the C6 atom and visible at 2921 cm^{-1}, is affected by the presence of HAp, as can be noted in the spectra of ED1-ED3, which display two further signals at 2978 cm^{-1} and 2890 cm^{-1} (Fig. 1). It should be emphasized that the hydrogen bonding between OH group of β-CD and Ca^{2+} ions of HAp, revealed by the intensity decrease of the band at 3270 cm^{-1} assigned to the OH group stretching (Fig. 1), is confirmed by the thermal decomposition behaviour of the composites (Fig. 4). In fact, the composites with the most pronounced attenuation of 3270 cm^{-1} band are those with the lowest mass loss - this could thus be attributed to a higher density of hydrogen bonds in ED2 and ED8 composites.XRD analysis is most suitable for identification of crystallographic structure and providing the crystallinity index as well. XRD pattern of the composite ED1, reported in Fig. 2 as an example, reflects the formation of β-CD/HAp composites with an average crystallite size ranging from 46 to 74 nm (Table S2).

The peaks attributable to the β-CD component [57] at 2θ values are visible at 9.71°, 10.6°, 12.4°, 15.3°, 16.04°, 17.6°, 18.8°, 19.5°, 20.6°, 22.6° and 27.02° for all the composites. HAp diffraction peaks at 25.9°, 28.3°,29.1°,31.8°,32.2°,32.8°,34.2°, 39.9°, 42.1°, 43.9°, 45.5°, 46.7°, 48.2°, 49.6°, 50.5°, 51.3°, 52.2° and 53.3° are attributed to the (002), (102), (210), (211), (112), (300), (202), (310), (311), (113), (203), (222), (312), (213), (321), (400), (402) and (004) planes, according to the literature [58]. However, the peaks attributable to β-CD become broader and flatter between 7° and 12°, and this remains valid for the HAp characteristic peaks at 25.9° and 31.8° This indicates that HAp is poorly crystallized when the amount of β-CD increases. A similar trend has been reported in the literature, with β-CD becoming part of a distorted HAp-based structure [59].

Scanning Electron Microscopy (SEM) is used to identify and characterize the morphology and structure of composite materials The SEM micrographs of β-CD, HAp, and ED1 composite are reported in Fig. 3 for comparison. The surface of ED1 composite (Fig. 3a) presents a rough, heterogeneous morphology, dominated by numerous agglomerated bundles of nanorod-like structures. This dense clustering suggests strong intermolecular interactions within the composite, potentially enhancing its mechanical stability and surface area. The β-CD sample (Fig. 3b)

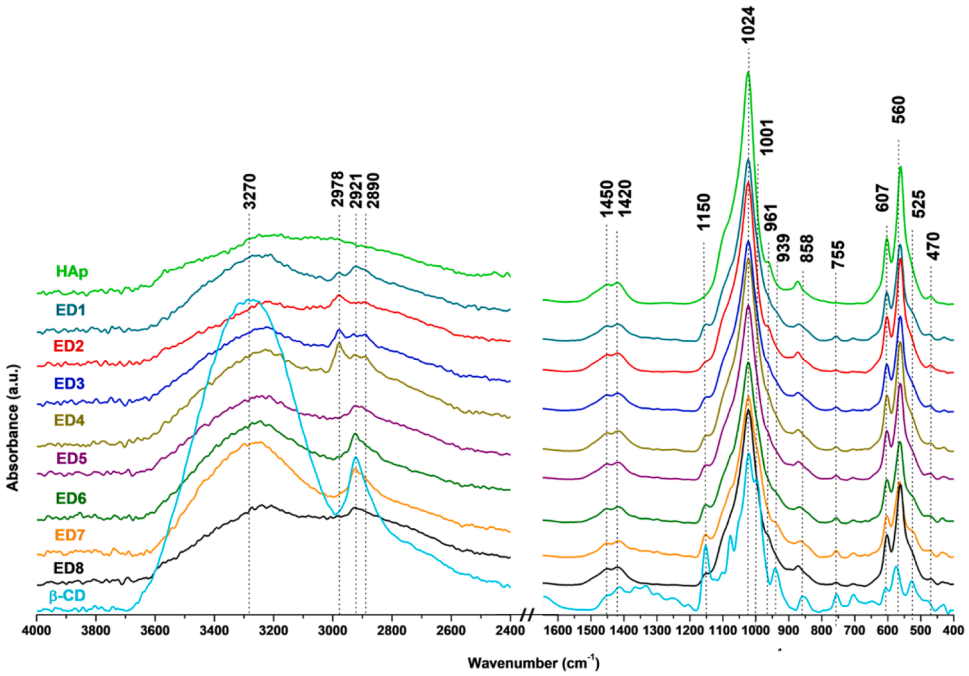

Fig. 1. Left: ATR-FTIR full spectra of β-CD, ED1-ED8 and HAp; right: expansion of the ATR-FTIR spectra in the region 650–900 cm^{-1}; top: expansion of the ATR-FTIR spectra in the region 4000–2400 cm^{-1}.

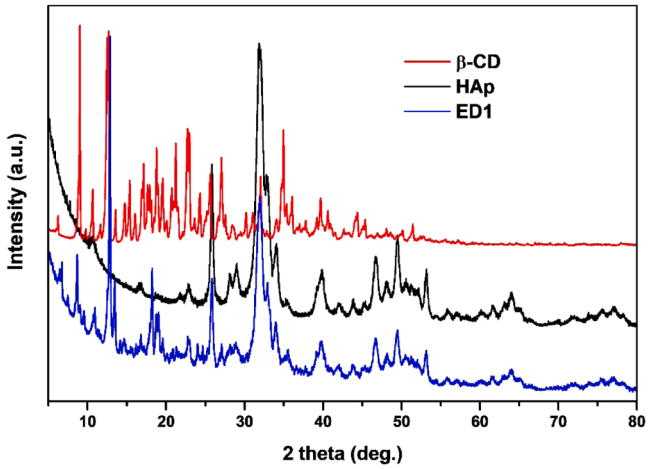

Fig. 2. From bottom to top, XRD spectra of ED1 (blue), Hap (black) and β-CD (red).

exhibits a contrastingly smooth and flat surface with well-defined channels running throughout. This ordered morphology hints at a crystalline-like arrangement, which could aid in controlled molecular encapsulation or adsorption due to the material's uniformity. Contrarily, the HAp sample (Fig. 3c) displays a distinctive porous morphology, characterized by dispersed nanorods across the entire surface. This porosity indicates significant internal voids within the material structure, likely enhancing the material's capacity for adsorption or interaction with external molecules.

2.1.3. *Thermal analysis of β-CD/HAp composites*

Thermogravimetry is a technique in which the mass of the sample is monitored against time or temperature while the temperature of the sample, in a specified atmosphere, is programmed. This measurement offers data on physical events such as adsorption, desorption, as well as chemical phenomena such as chemisorption, thermal breakdown, and solid-gas interactions (e.g., oxidation or reduction). The complete set of TGA curves for the ED1-ED8 composites are shown in Fig. 4. The results of the TG, DTG and DTA curves for HAp, β-CD and ED1-ED8 composites are presented in Supplementary Materials (Figure S2-S4).

For β-CD/HAp nanocomposites (Fig. 4), a first step of weight loss (up to about 200 °C) was due to the evaporation of the absorbed/adsorbed water on both HAp and β-CD molecules [60], as well as to NH_3, most probably arising from the HAp synthesis [17]. Two further main steps of mass loss in the 300 – 600 °C temperature region, related to the thermal degradation (at about 300 °C) and oxidation (at about 500 °C) of β-CD glucose units [61], were observed and are consistent with the data reported by Gowri [42]. A slight weight loss at about 800 °C with a release of the constitutional water from HAp, following the conversion of HAp into oxyhydroxyapatite and further conversion to calcium triphosphate [62], was also observed. The main and abrupt mass loss steps attributed

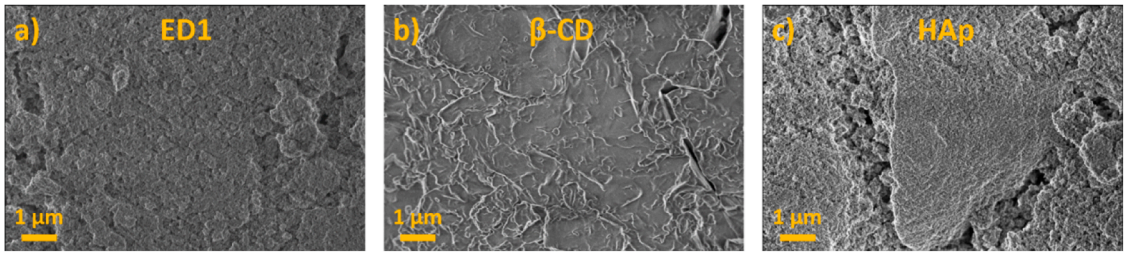

Fig. 3. SEM images of the a) ED1 composite, b) β-CD sample, and c) HAp sample.

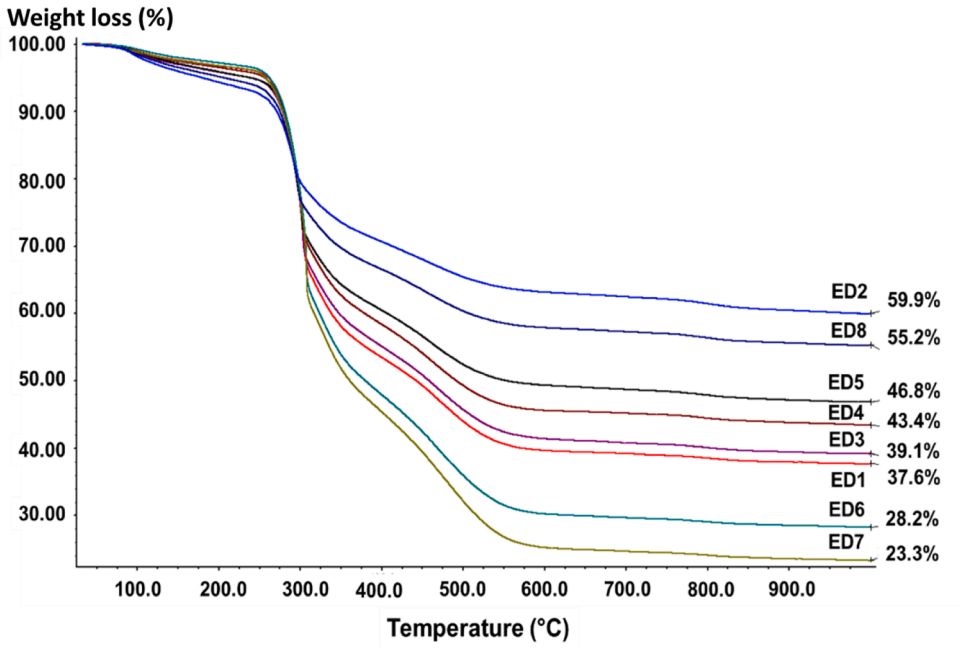

Fig. 4. Overlay of TGA curves for the ED1-ED8 composites.

to thermal degradation at about 300 °C occurs at the same temperature for all composites (the overlay of TG curves in this region is almost perfect), suggesting that the compositional and structural changes didn't induce any alteration of their decomposition temperature. Regardless of the ratio β-CD/HAp, β-CD has the greatest contribution to the composites' total mass loss (as it is almost totally decomposed at 1000 °C), while HAp has only a minor contribution (as it loses only 17 % of mass at that temperature). Thus, the total mass loss of the composites is mainly related to the amount of β-CD and, as expected, the greatest mass loss (and the lowest final residue, correspondingly) was found for samples ED7 and ED6 (with β-CD:HAp synthesis ratios of 3:1 and 2:1, respectively). It is interesting to note how the trend in composites' weight loss (Fig. 4) follows the trend in their average sizes and ZP values, with the exception of ED1 and ED3, which are highly unstable, and ED6 and ED7, for which ZP values were not detectable. Composites are less likely to undergo significant structural changes the more stable they are. It is also worth noting that the hydrogen bonding between OH group of β-CD and Ca^{2+} ions of Hap revealed by the intensity decrease of the band at 3270 cm^{-1} assigned to the OH group stretching (Fig. 1) is confirmed by the thermal decomposition behaviour of the composites (Fig. 4). In fact, the composites with the most pronounced attenuation of 3270 cm^{-1} band are those with the lowest mass loss - this could thus be attributed to a higher density of hydrogen bonds in ED2 and ED8 composites.

2.1.4. *Cytotoxicity and antimicrobial activity of β-CD/HAp composites*

Leather contact directly or indirectly with the human skin, making it important to evaluate its cytotoxicity, Moreover, leather is a naturally hydrophilic material that offers a potential medium for the growth of microorganisms, hence it is critical to enhance the material's long-lasting antimicrobial effects by fixing antimicrobial agents in the leather structure.

The cytotoxicity test measures the cell death caused by a specific material or the percentage of viability before and after exposure to the specific material [63]. The cytotoxicity tests conducted on the β-CD/HAp composites assessed LDH release (plasma membrane damage) and cell viability (MTT assay). No statistically significant LDH release (Figure S5) was observed compared to control after 48 h of incubation. The results of MTT assay (Figure S6) were in agreement with the LDH release, since the number of viable cells did not decrease >12 % from control, proving the biocompatibility of the HAp-based composites. The antimicrobial activity against most common bacteria species populating human derma is highly desirable. The composites have tested and shown a marked antimicrobial activity against *Staphylococcus aureus, Escherichia coli, Brevibacterium lines and* Staphylococcus epidermis, as can be seen in Tables S3-S4, most probably due to the presence of HAp [64,65]. It should be mentioned that *Brevibacterium linens* is ubiquitously present on the human skin, where it causes foot odour. *Staphilococcus epidermidis* generally resides benignly on the skin, with infections arising most commonly in compromised patients, including drug abusers, patients on immunosuppressive therapy, patients with AIDS, premature neonates, and patients with an indwelling device such as a catheter or implant. Once systemic, *S. epidermidis* can cause sepsis and a number of other detrimental conditions, including native valve endocarditis, or other subacute or chronic conditions in susceptible patients. These outcomes are very encouraging, as the composites here reported can be potentially incorporated into leather that may come into contact with human skin.

2.2. *Interaction of newly synthesized composites with collagen matrix: laboratory experiments*

2.2.1. *Effect on collagen matrix thermal stability*

Leather thermal stability is one of the most crucial aspects of the leather tanning process. It is mainly depending on the type of tannin used to tan the hides. This property could benefit from the use of a re-tanning agent. We therefore investigated the ability of the new composites to interact with collagen and increase its thermal stability using two approaches targeting the microscopic (i.e. fibers) and mesoscopic (i.e. fibrils) levels of the well-organized hierarchical multilevel structure of collagen.

Micro Hot Table (MHT) method is a method to evaluate the effects of tanning substances on collagen fibres' thermal stability. The stretch-induced microscopic fibre movements also called shrinkage activity, in relation to temperature increasing, defines the hydrothermal stability and structural heterogeneity of collagen fibres. Shrinkage temperature T_s is used as a metric to evaluate the quality of the tanning process [66] and refers to the starting temperature of the main shrinkage interval, while fT_s refers to the temperature at which the simultaneous shrinkage

of fibres is observed. T_{first} (T_f) and T_{last} (T_l) are defined as the temperatures at which the first and last shrinkage activity of an individual fibre is observed. In Table 3, the parameters of shrinkage activity for the hide powder (HP) treated with the new composites compared with those of the not-treated hide powder, are reported.

As expected, the hide powder samples treated with the new composites show higher T_s values compared to the not-treated one. The values are in good accordance with the DLS and Z-potential results, showing a stronger interaction of collagen matrix with ED2, ED5 and ED8 composites, namely those showing the best polydispersity values and suspension stability.

Micro-DSC in excess water provides a useful basis for the evaluation and description of fibrillar collagen thermal denaturation. It allowed us to identify and quantify the different collagen populations with distinct thermal stabilities for all hide powder-composite combinations, based on the fact that the percentage contribution of each endothermic component to the total denaturation enthalpy is proportional to the percentage of the corresponding collagen population [67–69]. The micro-DSC peak of the not-treated hide powder shows a main denaturation peak at $T_1 = 54.1$ °C, with a shoulder at $T_2 = 61.0$ °C (Figure S7). When compared to hide powders treated with our ED1-ED8 composites (Figure S7), we found that the ED2 and ED8 composites produced the best results, which were consistent with the MHT results. They exhibit a peak around 54 °C with a shoulder around 61 °C, representing the collagen populations of the chemically unmodified collagen within hide powder. The increase in the hydrothermal stability is demonstrated by the occurrence of a third collagen fraction denaturing at $T_3 > 63$ °C, representing about 10–14 % of the total collagen. This is the collagen which interacted with the composite, with a stabilizing effect on the collagen matrix. It is worth noting that of all the combinations, HP-ED2 and HP-ED8 have the highest denaturation enthalpies, indicating more structural stability than the others.

2.2.2. Changes on hide powder surface morphology

The SEM micrographs of the hide powder before and after the treatment with the ED8 composite (selected to be used in the pilot-scale experiments) are presented in Fig. 5. The not-treated hide powder (Fig. 5a) displays a fibrous-like surface morphology, with visible, elongated fibers that suggest a loose, open structure characteristic of natural hide material. This fibrous arrangement likely enhances the surface area, which could aid in interactions with other substances, but also implies lower structural density. Fig. 5b shows that the ED8 composite has a specific nanorod structure. After the treatment with ED8 composite, the hide powder's surface morphology is changed (Fig. 5c). It appears more cohesive and the nanorod structures of the composite are no longer observed. This indicates that ED8 composite effectively embeds into the fibrous structure, better connected them and potentially enhancing its properties.

2.3. Interaction of ED8 composite with collagen matrix: pilot-scale test

The composite ED8 was chosen for testing in the wet-white re-tanning process based on the following properties: nanoparticles average dimension, stability and polydispersity, char formation, proven interaction with collagen fibers, antimicrobial activity and lack of toxicity. Even though ED2 has demonstrated similar properties, the choice fell on ED8 because of its lower cost ensured by a higher concentration of hydroxyapatite than the more expensive cyclodextrin.

ED8 was applied during the wet re-tanning process as reported in Table S6 and the properties of the leather specimen obtained were compared to a leather specimen obtained through a similar technology (Table S5), except the adding of ED8. The obvious features that differentiate the two specimens of leather are the colour, feel and appearance of the surface as depicted in Fig. 6. The treated leather is "filled" by the re-tanning relatively large scale composites and hence looks and feels fuller (Fig. 6a) compared to the not-treated leather (Fig. 6b). This perceived quality of the ED8-treated leather is most likely due to the ability of the composite to improve dye's penetration and act as a filler. Actually, the UNI EN ISO 105- B02:2014 test for the Colour fastness to artificial light confirms that the composite improves colour stability. This can be easily explained by the presence of the β-CDs, which are extensively used as auxiliary agents in dyeing and as a matrix for dye adsorption [70]. The filling effect is confirmed by the significant increase in thickness (Table 7). This is most likely due to two reasons: (i) cyclodextrins are quite accommodative to water molecules [71] and (ii) water molecules form a dense and structured layer around the HAp molecules, with small-sized particles posing greater interaction energy with water molecules than the large-sized particles [72]. Anyway, increase in thickness is also related to a huge surface binding of composites. This last contribution can't be neglected. Indeed, micro-DSC measurements show that only 11.8 % of the total collagen in the sample interact with ED8, resulting in a higher stability collagen population (as from Table 4, last raw and last column, i.e., percent of ΔH_3.) Furthermore, the UNI EN ISO 3380: 2015 standard test confirms the collagen matrix hydrothermal stabilization by an increase in the shrinkage temperature by 6.5 °C, in agreement with the results obtained at laboratory scale by MHT method, hinting at a mild penetration of composites inside the leather or a different interaction of composites with collagen fibrils and fibers (Table 5).

By comparing the micro-morphology of the two specimens of leather illustrated in Fig. 7 it appears that the treated leather shows micro-cracks (Fig. 7c) and a higher coating power of the surface fibers (Fig. 7d). Such micro-cracks could be attributed to the difference between the mechanical properties of the HAp and collagen fibers which can create discontinuities in the collagen-composite matrix structure due to temperature and humidity variations experienced during hide processing. On the other hands, these micro-cracks may have a beneficial effect on leather breathability.

The NMR Mouse® devices have started to be increasingly used in biological and material science [73]. Liquid-phase relaxation times are, in fact, susceptible to post-treatment modifications in a porous structure [74]. In fact, the transverse relaxation time, T_2, can be related to how water molecules associate with collagen in different phase, namely amorphous and crystalline phases [75]. Specifically, short transverse relaxation time (T_{2A}) correlates with the rigid phase of collagen, indicating the structural water which is not influenced by the changes in the final structure, while medium and longer relaxation time (T_{2B}, T_{2C} and T_{2D}) can be associated with the amorphous state [66,76].

As reported in Fig. 8 and Table 6, the value of T_{2A} doesn't change too much, when we compare the non-treated with the ED8-treated leather. Nevertheless, T_{2B} and T_{2C}, strictly related to the amorphous phase of the collagen, decreased after the treatment with ED8, suggesting a reduction in the molecular mobility due to collagen-ED8 interaction. The presence of a further component T_{2D}, could be related to the presence of the composite on the leather structure [35].

On the other hand, the increase in T_1 apparently might seem to be at odds with the increase in thermal stability since artificially ageing experiments demonstrated that an increase of spin-lattice T_1 relaxation

Table 3
Shrinkage parameters of hide powder treated with the newly synthesized composites compared to those of not-treated hide powder.

Sample	T_f (°C)	T_s (°C)	fT_s (°C)	T_l (°C)
Hide powder (HP)	40.3	56.4	66.6	78.4
HP-ED1	46.8	58.6	71.6	80.6
HP-ED2	55.5	65.3	73.4	84.0
HP-ED3	43.6	61.6	67.0	75.7
HP-ED4	51.8	63.0	72.0	85.2
HP-ED5	51.2	60.1	72.7	80.1
HP-ED6	52.7	60.2	67.6	77.8
HP-ED7	55.1	62.7	68.7	80.0
HP-ED8	52.2	63.6	73.6	85.9

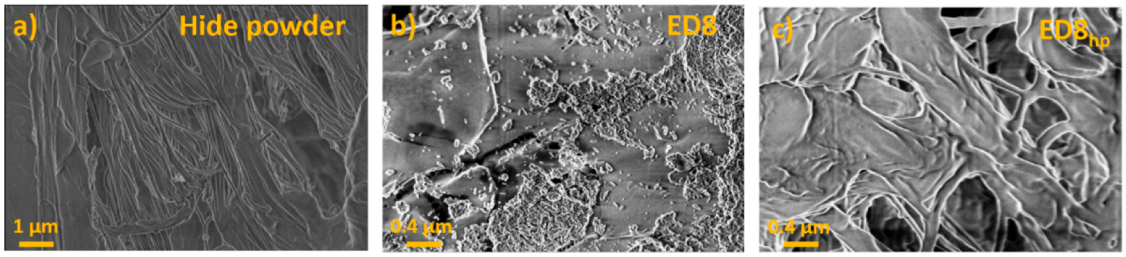

Fig. 5. SEM images (magnification at 20 kX) of the a) hide powder, b) ED8 composite, c) hide powder treated with ED8.

Fig. 6. Surface aspect of ED8-treated leather (a) compared to that of the not treated leather (b).

time is attributable to the progressive thermal destabilisation of tanned collagen [77]. As previously reported by some of us, the T_1 value of leather is a measure of the strength of water-mediated bonding in the collagen matrix, depending on the number of sites capable of strong interactions with water, which, in turn, depends on both the chemical structure of tannin and the micromorphology of collagen in the animal hide [66,77]. In the case of ED8-treated specimen, we are dealing with an additional re-tanning agent, with a different chemical structure, whose insertion/interaction with the collagen matrix might produce a disturbance evidenced by the variation of T_1. This explanation is supported by the fact that we found similar T_1 values when HAp was added as flame retardant additive in the wet re-tanning process [78].

TG/DTG/DTA analysis was also performed (Fig. 9) to compare the thermal stability of the two leather specimens.

From the TG/DTG/DTA curves, three main degradation processes can be detected in both samples: i) the first mass loss related to water release; ii) the decomposition at about 320 °C related to collagen matrix thermal decomposition; and iii) a second decomposition at around 550 °C corresponding to strong thermo-oxidation [79]. Unlike the not-treated leather, the ED8-treated leather continued to lose mass on heating up to ≈ 800 °C, indicating the presence of other thermally unstable residues [80], most probably from ED8 composite. Although the addition of the composite has little effect on the temperature of maximum mass loss of the second process (only 3 °C increase), there is a slight shift of the third mass loss to higher temperatures (about 20 °C), indicating a delay of the thermo-oxidation process.

X-ray diffraction is a widely used technique to understand the structure of collagen in biomaterials [81]. Small and wide-angle X-ray diffraction was used to measure quantitatively the changes induced at the nanoscopic and microscopic levels of collagen during manufacture of parchment from animal skin [82]. As the first physical and chemical processes in parchment manufacturing (i.e. salting and liming) are the same as in the process of making leather, such insight could be used as a guide for optimising the industrial leather making process. Synchrotron-XRD (SXRD) patterns collected at ambient conditions for the not-treated and ED8-treated leathers are shown in Fig. 10. Both patterns consist of three characteristic peaks located at 2θ ~ 7°, 20° and 31° typical for a collagen structure, corresponding to the intermolecular lateral packing of collagen molecules (peak '1′), amorphous component (peak '2′), and periodicity of the axial rise by residual (peak '3′) [82]. Few faint peaks recognised only in the treated leather SXRD pattern are marked with an asterisk symbol. Those peaks might be assigned to minor traces of ED8 composites. Nevertheless, it can be concluded that the composites presence in the treated leather after the wet-finishing process (Table S5-S6) is barely detectable (i.e. at the edge of detection limits) by SXRD (< 1 %).

The changes associated with the irreversible thermal denaturation of collagen structure in the not-treated and ED8-treated leathers were also followed and qualitatively compared employing *in-situ* temperature SXRD measurements. Fig. 11 shows the temperature evolution of diffraction patterns for both the not-treated and treated leather specimens during heating and cooling between room temperature and 250 °C. Collagen peaks at ~ 7° and 31° gradually disappear as temperature increases, as expected. Denaturation is not a reversible process; therefore, these peaks do not reappear when the specimens are cooled back to ambient conditions.

To demonstrate it clearly, the normalised peak '1′ area was plotted in Fig. 12 as a function of temperature for both leather specimens, i.e., ED-8 treated and not-treated. The temperature dependence of the two curves is remarkably similar, as expected. The peak '1′ area remains somewhat stable until the temperature roughly reaches 80 °C, when a significant and steep decrease begins. This decrease considerably slows down by around 150 °C, and by 250 °C, the peak "1″ areas are merely a tiny portion of their preheating values. This is consistent with fundings from previous studies on collagen thermal denaturation: the collagen crystalline phase denatures at temperatures higher than 210 °C, while the less stable amorphous phase denatures in the range (50 – 120) °C, depending on the hydration level of the collagenous material [83]. Actually, during the SXRD experiment, leather underwent simultaneous dehydration and denaturation, in agreement with both thermal analysis results, which indicate that first dehydration process takes place in the range 80–100 °C, and MHT results, which show shrinkage occurring at 70–80 °C. Starting from 80 °C, thermal denaturation takes precedence over the dehydration process, which is why the area of peak 1 decreases very abruptly, until most of the collagen (the less thermally stable, or amorphous, fraction) completely denatures. Then, the more thermally stable fraction with very low hydration level (the so-called crystalline fraction) starts to denature, a process which is completed in the temperature range (220 – 250) °C.The peak '2′ that reflects the collagen amorphous component shifts to lower 2-theta values till 250 °C and then

Table 4
Thermal denaturation parameters of hide powder treated with ED1-ED8 composites compared to those of not-treated hide powder measured by micro-DSC in excess water.

Sample	T_{onset} (°C)	$T^a_{max\ i}$ (°C)	$\Delta T_{1/2}$ (°C)	$\Sigma\Delta H^a_i$ (J·g^{-1})	% ΔH^a_i
Hide Powder (HP)	49.5	T_1= 54.1 T_2= 61.0	5.9	35.4	ΔH_1= 74.4 ΔH_2= 25.6
HP-ED1	49.3	T_1= 53.0 T_2= 60.2	4.9	13.9	ΔH_1= 84.1 ΔH_2= 15.9
HP-ED2	50.2	T_1= 54.2 T_2= 61.2 T_3= 66.0	5.6	16.3	ΔH_1= 77.3 ΔH_2= 12.8 ΔH_3= 9.9
HP-ED3	50.0	T_1= 54.1 T_2= 59.8	4.6	10.4	ΔH_1= 80.1 ΔH_2= 19.9
HP-ED4	47.9	T_1= 52.2 T_2= 59.2 T_3= 65.5	5.7	10.2	ΔH_1= 74.4 ΔH_2= 16.1 ΔH_3= 9.5
HP-ED5	48.1	T_1= 52.3 T_2= 58.9 T_3= 64.2	5.8	13.1	ΔH_1= 70.8 ΔH_2= 14.9 ΔH_3= 14.3
HP-ED6	49.0	T_1= 52.9 T_2= 59.3 T_3= 63.7	4.9	8.3	ΔH_1= 81.1 ΔH_2= 14.2 ΔH_3= 4.7
HP-ED7	48.6	T_1= 52.4 T_2= 59.1	5.4	11.2	ΔH_1= 87.2 ΔH_2= 12.8
HP-ED8	50.5	T_1= 54.6 T_2= 61.0 T_3= 65.5	5.0	17.6	ΔH_1= 73.7 ΔH_2= 14.4 ΔH_3= 11.9

i = 1–3 index of the collagen population with distinct hydrothermal stability.

Table 5
Results of the standard tests applied to ED8-treated leather and not-treated leather.

Sample	Not treated leather	ED8-treated leather	Standard method
T_s[a] (°C)	72.0 °C	78.5 °C	UNI EN ISO 3380: 2015
Thickness[b] (mm)	1.66 mm	2.23 mm	UNI EN ISO 2589: 2016
Colour fastness[c] (grey scale)	2/3 (24 h) 2/3 (48 h) 2 (72 h)	3/4 (24 h) 3/4 (48 h) 3 (72 h)	UNI EN ISO 105-B02:2014 Xenon arc fading lamp test

(a) T_s = Shrinkage temperature: https://www.iso.org/standard/61792.html. (b) ISO 2589:2016 specifies a method for determining the thickness of leather. The method is applicable to all types of leather of any tannage. https://www.iso.org/standard/68859.html. (c) ISO 105-B02:2014 specifies a method for determining the effect on the colour due to the action of an artificial light source representative of natural daylight (D65): https://www.iso.org/standard/65209.html.

moves back to higher 2-theta because of a thermal expansion/compression. The shape of this peak may alter as a result of the heating/cooling process, becoming narrower and more symmetric. Again, the observed changes are very similar for both not-treated and ED8-treated leather specimens. It should be mentioned that collagen fibrils in cow hide, are linear arrangements of collagen monomers which comprise hundreds of molecules in their cross-section of about 150 nm in diameter [84]. The peak related to ED8 composite at ~ 29° (Table S7) disappear at 200 °C. This might be attributed to the fact that ED8 interact with the amorphous fraction of collagen which is fully denatures up to 200 °C.

ATR-FTIR analyses were also performed on the leather specimens exposed to *in-situ* heating to evaluate how the heating modified their molecular structure. As previously reported by Cappa *et al.* [85], the changes in the amide I (1640 cm^{-1}), amide II (~1550 cm^{-1}) and amide III (~1340 cm^{-1}) bands are not so evident even after collagen was dry heated at 200 °C for 6 h. In fact, no evident shifts of amide bands were observed after the heating of both leather specimens (Fig. 13), whereas evident changes occurred in the region of carbohydrate (collagen proteoglycans) moieties (C–O stretching and C–O–C stretching) [86], with the not-treated leather showing more significant alterations at 1142 and 1103 cm^{-1} (Fig. 13). The increase of these two bands after heating might be attributed to the release of proteoglycans as a result of thermal denaturation. The spectral features are thus consistent with ED8 thermally stabilizing the collagen matrix.

3. Materials and methods

β-cyclodextrin (β-CD) was purchased from Roquette (Kleptose® GC grade ≥ 93 %) and used without further purification. The synthesis of HAp particles was performed according to the procedure developed by University of Turin and Kemia Tau within the M-Eranet project InSuLa Innovative materials and technologies for sustainable leather manufacturing for automotive [78]. Industrial grade hydrated lime, phosphoric acid 85 % and NH_3 solution 33 % were used for the synthesis.

The ultrasound experiments were performed with a Sonic Vibracell VCX 750 ultrasonic liquid processor equipped with a 13 mm titanium probe. The mixing of the two precursors, β-CD and HAp was carried out in a glass flask at atmospheric pressure. To avoid the temperature rise in the reaction vessel, a cooling mixture of water/glycol at 15 °C was circulated in the reaction vessel jacket by a Thermo Scientific HAKEE G50 refrigerated circulator.

Laboratory tanning tests on hide powder were performed at the Leather and Footwear Research Institute (ICPI), the research Branch of the National Research and Development Institute for Textiles and Leather (INCDTP), Bucharest. The hide powder used was SLTC Official hide powder batch B60 purchased from BLC Leather Technology Center Ltd., England. T500 mg hide powder was soaked in 7.5 mL distilled water in which 60 mg of NaCl was added and stirred for 30 min at 30 °C. Then, 200 mg of β-CD/HAp composite (ED1-ED8) was added and stirred at 30 °C for 24 h Finally, the suspension was filtered through a fast filter paper and left to dry at room temperature.

Calf hides used for the pilot scale test were made available by the A3 Leather Innovation Center from University of Lleida (UdL). The study was carried out using raw hides processed from the beamhouse to tanning. The selected β-CD/HAp composite was added during the retanning stage prior to drying and finishing as reported in the Supplementary Materials (Table S5-S6).

3.1. Analyses methods and techniques

A Malvern Nanoseries Zeta Sizer was used to perform Dynamic Light Scattering (DLS) and measure the hydrodynamic size of the composite particles and the Zetapotential of their suspensions. All the samples were diluted with double distilled water (1mg/100 mL) and filtrated before

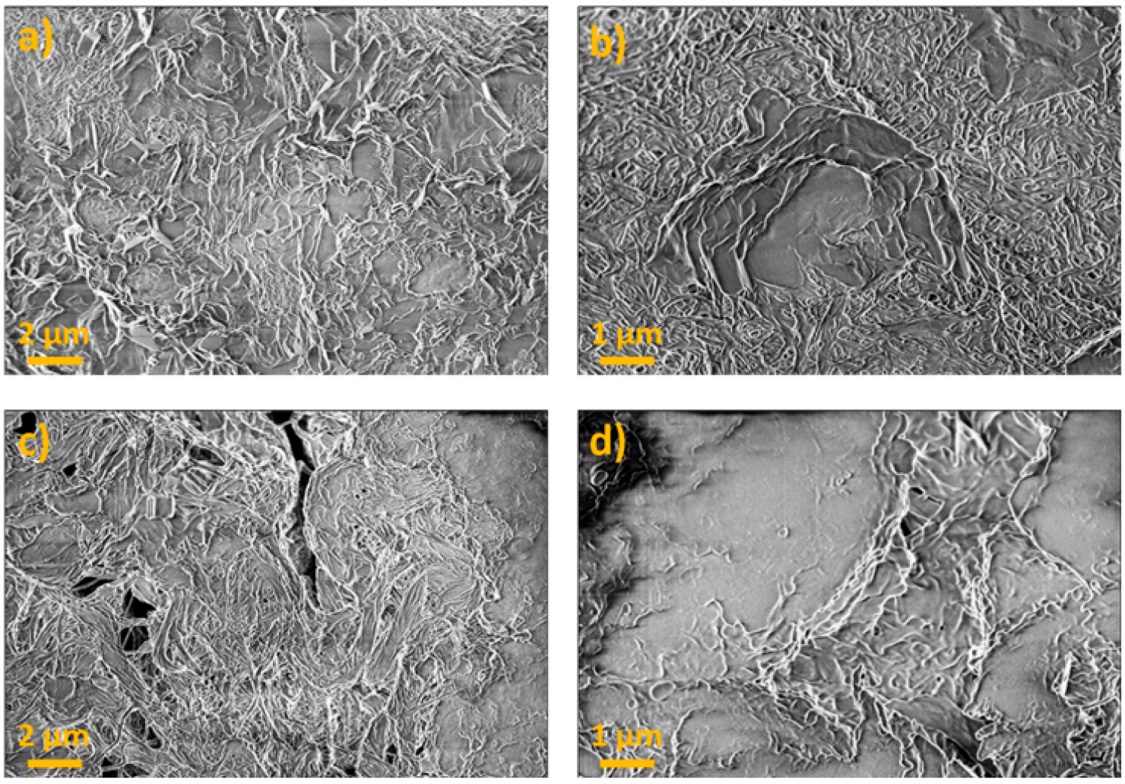

Fig. 7. SEM images of the not treated leather with a) 5.00 K and b) 10.00 K magnification compared with those of ED8-treated leather with c) 5.00 K and d) 10.00 K magnification.

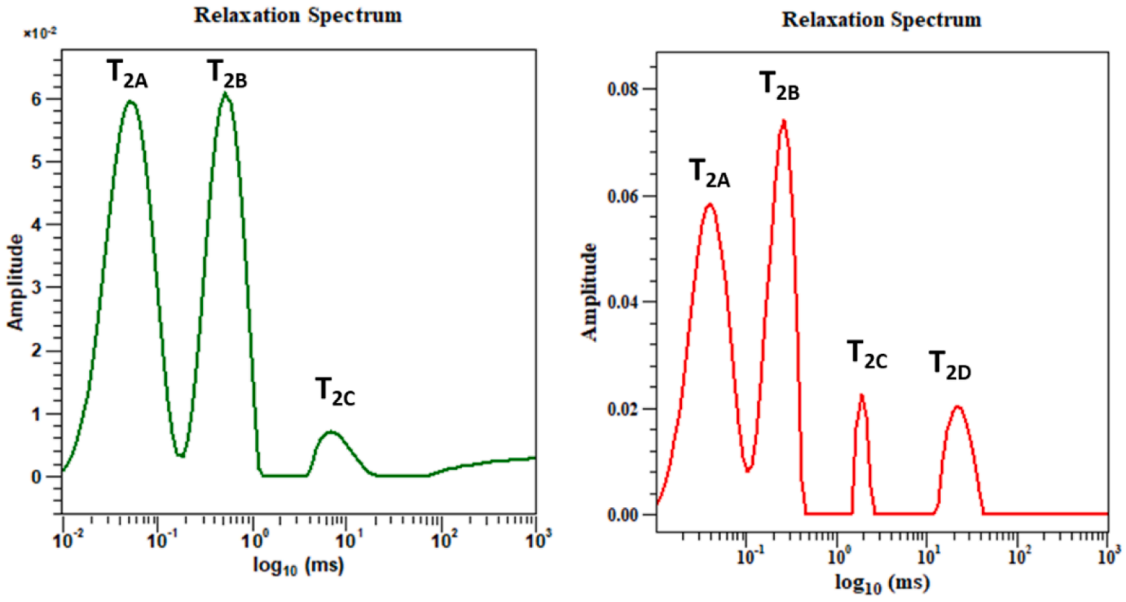

Fig. 8. ^{1}H CPMG transversal relaxation time (T_2) distribution calculated with the inverse Laplace transform for not treated (green) and ED8-treated (red) leathers.

Table 6
NMR MOUSE® relaxometric parameters of not treated and ED8-treated leathers.

Sample	T_1	T_{2A}	T_{2B}	T_{2C}	T_{2D}
Not treated leather	19.6	0.05	0.52	6.73	–
ED8-treated leather	25.9	0.04	0.26	1.87	21.54

the measurements. All experiments were performed in triplicate.

X-ray diffraction data (XRD) of the β-CD/HAp composites were acquired in the 2θ range 5°−60° using a PANalytical X'Pert MPD diffractometer (40 mA, 45 kV) with the Cu- Kα1 radiation (λ = 1.5406°A) working in the Bragg–Brentano geometry. During XRD measurements the 2θ step size was 0.02° and the acquisition time was 20 s/step. Data processing was performed using HighScore Plus software 4.8 and PDF-4+ Database.

The XRD data of β-CD and HAp were analyzed by selecting the peaks with the highest intensity for each compound. Further, Scherrer formula

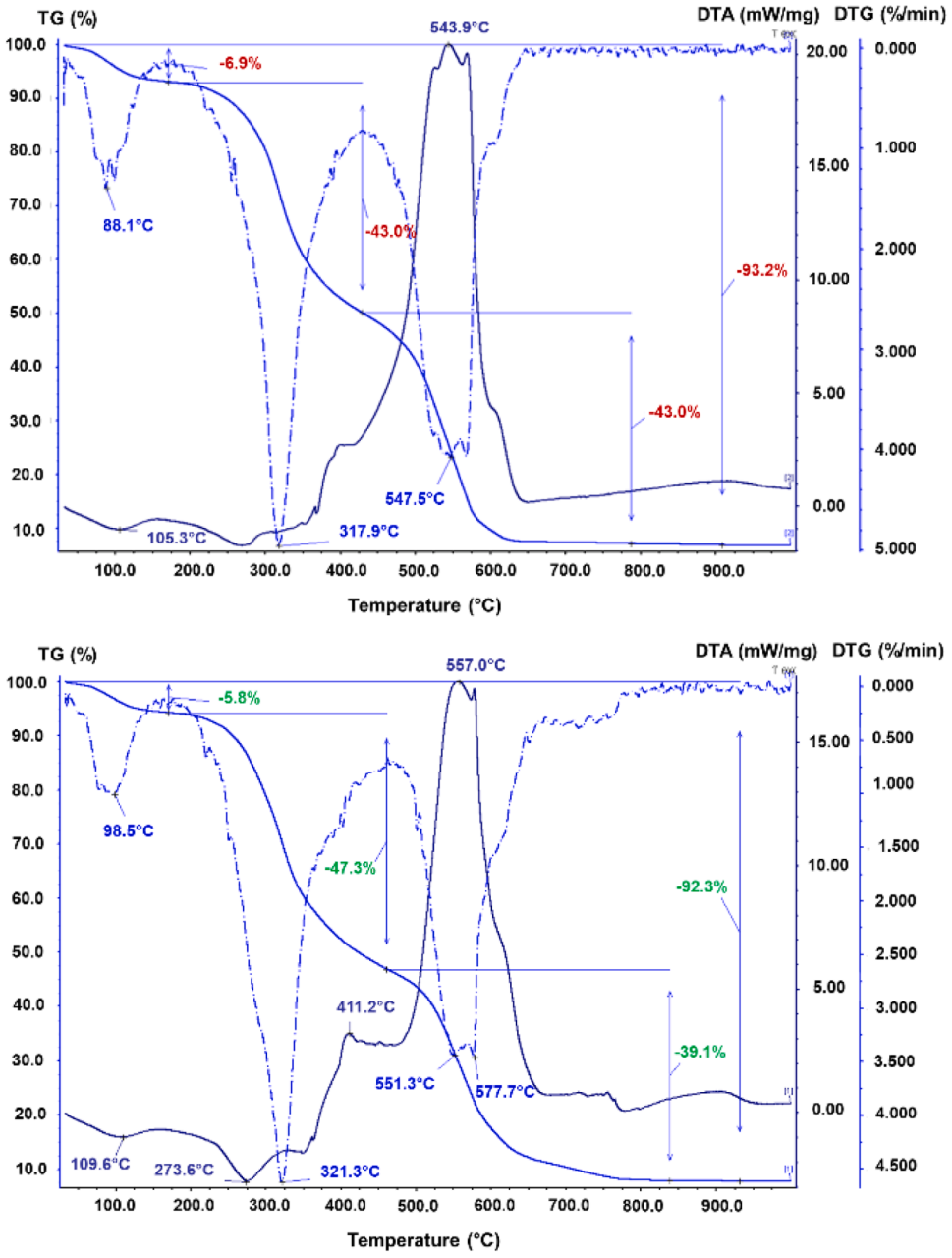

Fig. 9. TG (full line blue) /DTG (dotted line blue) /DTA(full line black) of not-treated leather (top) and the ED8-treated one (bottom).

(1) was used to calculate the dimensions of the crystallites (grains) and the lattice strain.

$$Dp = (0.94 * \lambda) \ / \ (\beta * Cos\theta) \quad (1)$$

Where:

Dp = Average Crystallite size,

β = Line broadening in radians (FWHM),

θ = Bragg angle,

λ = *X*-Ray wavelength.

The Infrared Spectroscopy in Attenuated Total Reflection mode (ATR-FTIR) analyses were carried out using an ALPHA spectrometer (Bruker Optics) equipped with a Platinum ATR module. The penetration depth, depending on the refractive indices of ATR crystal and sample, typically amounts to a few microns (ca. 0.5–3 μm). Spectra were recorded in the 4000–400 cm^{-1} spectral range with a 4 cm^{-1} resolution, using 32 scans. Opus software (Bruker Optics, Germany) was used for the acquisition and elaboration of the spectra.

Simultaneous thermogravimetric (TG), derivative thermogravimetric (DTG) and differential thermal analysis (DTA) curves were recorded with the STA 409 PC instrument (Netzsch, under synthetic air flow (50 mL·min^{-1}), in the temperature range (25–1000) °C, at a heating rate of 10 °C min^{-1}. The mass of the analysed samples was in the range (10–15) mg. The evolved gases from thermal decomposition were analysed with a coupled Bruker Tensor 27 FTIR spectrometer equipped with a TG-IR gas cell. The FTIR spectra were collected continuously during measurements in the wavenumber range 4000–650 $cm^{-1}$with a resolution of 4 cm^{-1}. The identification of the evolved species was performed according to the public NIST database [NIST Chemistry Webbook Standard Reference Database No 69 (http://webbook.nist.gov/chemistry)].

Micro Hot table (MHT) measurements were performed with an equipment composed of a Linkam LTS120 micro heating plate (Linkam Scientific Instruments) equipped with an automatic heating rate adjustment system and a SMZ 745 Nikon stereomicroscope coupled to a

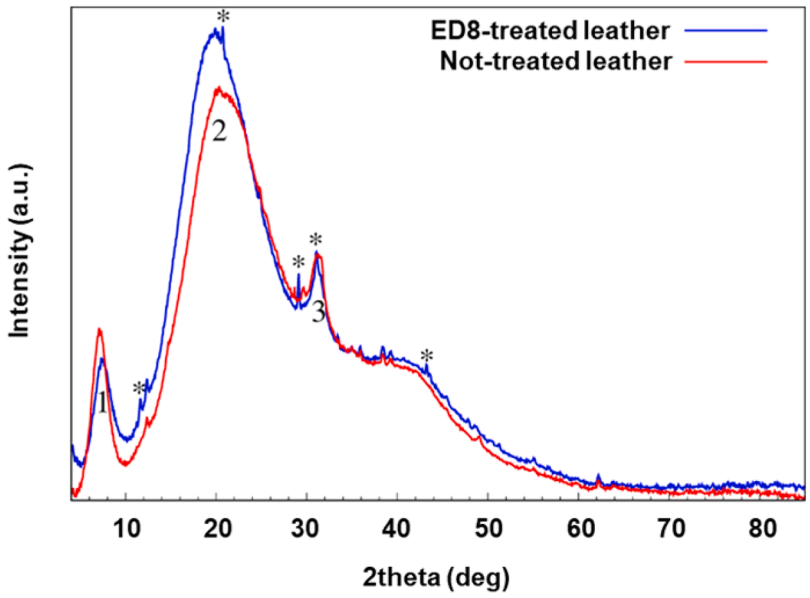

Fig. 10. SXRD patterns of the not-treated leather (red) and ED8-treated leather specimen with (blue) at ambient conditions before heating/cooling. Labels '1′, '2′ and '3′ mark the three main peaks related to collagen structure visible in both samples and asterisk labels '*' mark those peaks present only in the treated leather specimen.

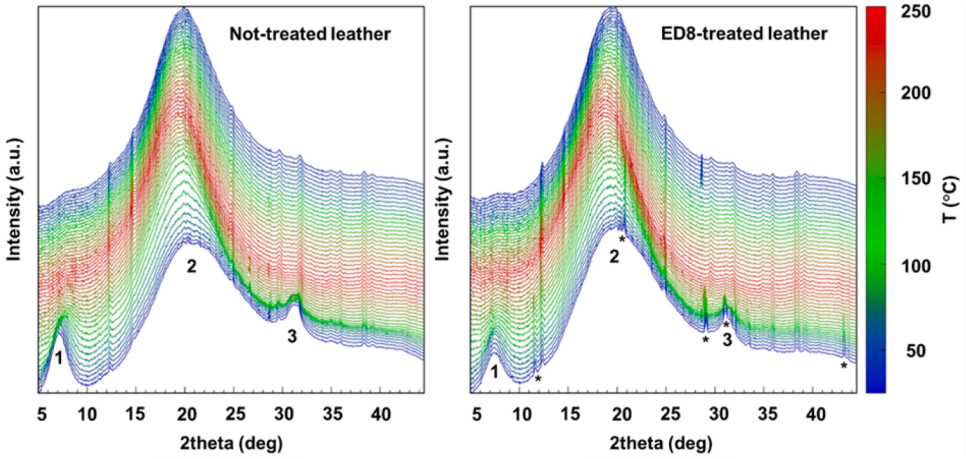

Fig. 11. In-situ SXRD patterns of the not-treated leather specimen (left) and treated leather specimen (right) collected during heating/cooling between room temperature and 250 °C. The curve colour reflects the temperature of data collection (colour bar on the right side).

Nikon D90 digital camera. Micro-samples of 10–15 fibres were thoroughly wetted and separated in demineralized water, placed on a microscope slide with a concavity and left 2 min to reach a homogeneous hydration level. The hydrated fibres were separated as much as possible under the microscope light using a pair of fine needles and then covered with a cover glass, placed on the hot table and heated at 2 °C·min^{-1}. The shrinkage process was digitally recorded, and the various temperatures defining the shrinkage activity were visually determined.

Micro-Differential Scanning Calorimetry measurements were carried out with a high-sensitivity Micro-DSC III calorimeter (SETARAM), in the temperature range (25–85) °C, at 0.5 °C min^{-1} heating rate, using 850 μL Hastelloy C cells. This low scan rate was applied to provide the quasi-equilibrium condition for DSC analysis and accurately measure the denaturation parameters. Samples of about (5.0–10.0) mg were suspended in 0.5 M acetate buffer (pH = 5.0) directly in the measure cell and left for 30 min to assure their fully hydration and avoid T_{max} and enthalpy variation with hydration level. Experimental DSC data acquired with the SETARAM SetSoft2000 software were analysed using PeakFit 4.1 (Jandel Scientific). DSC multiple peaks of the investigated samples were deconvoluted using the PeakFit asymmetric Gaussian fit function to improve the fit of the asymmetry in the peaks.

The morphological characteristics of the samples were analysed using a Gemini 500 Field Emission Scanning Electron Microscope (Zeiss).

The relaxometric behaviour of leather was measured using a ^{1}H unilateral NMR device (NMR-MOUSE® PM2, Magritek GmbH) controlled by a Kea 2 spectrometer and operating at 27.1 MHz. The ^{1}H spin-spin (transverse) relaxation times T_2 were measured using the Carr-Purcell-Meiboom-Gill (CPMG) pulse sequence (512 echoes) at a depth of 1 mm. The data obtained applying the CPMG pulse sequence were fit to the following function:

$$Y = \Sigma_{i=1}^{n} W_1 e^{\frac{-t}{T_{2i}}} \quad (2)$$

where n is the number of components used to fit the decay of the magnetization, W_i is the spin population of the ith component, and T_{2i} is the transverse relaxation time of the ith component.

The proton spin-lattice (longitudinal) relaxation times T_1 were

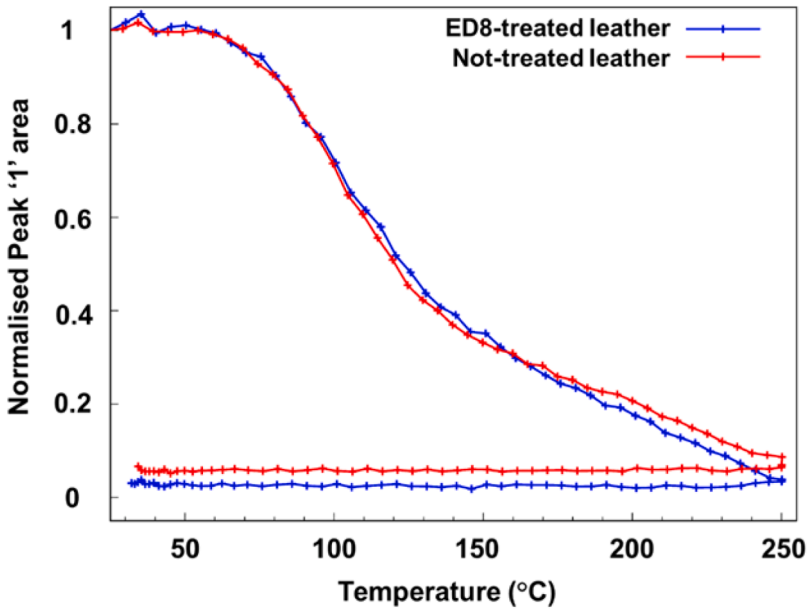

Fig. 12. Normalised area of the collagen peak '1′ as a function of temperature for ED8-treated (blue) and not-treated (red) leather specimens. Figure needs to be annotated to show where cooling is presented i.e. the flat lines of no change.

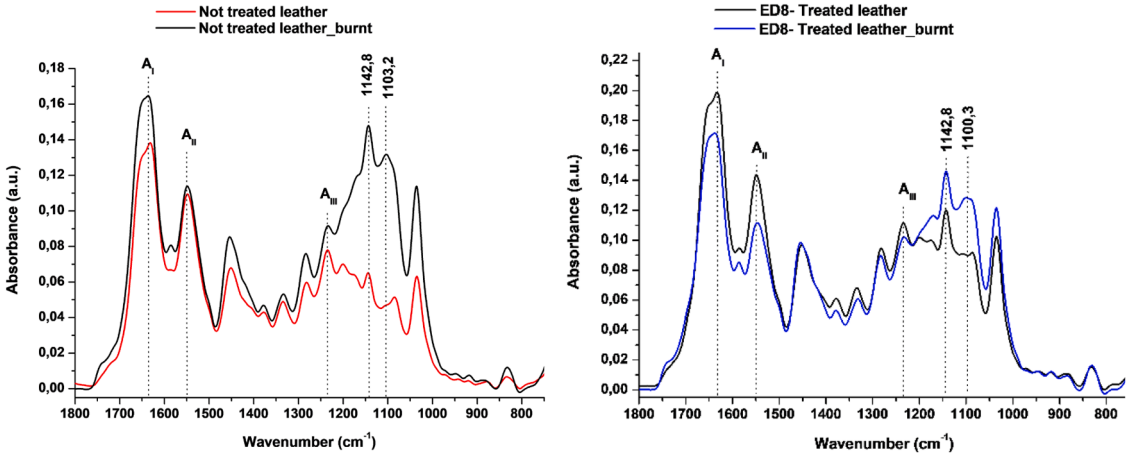

Fig. 13. ATR-FTIR spectra, in the region 1800–750 cm^{-1}, of the not treated (left) and ED8-treated leather before and after heating at 250 °C.

measured with the saturation-recovery pulse sequence using a Hahn-echo (32 echoes). The analysis of the saturation recovery data was best performed with the help of a single exponential function.

$$A(t) = A_{equilibrium}\left(1 - \exp\left(-\frac{t}{T_1}\right)\right) \quad (3)$$

The sum of spin populations was normalized to 100 %.

In-situ synchrotron-based X-ray diffraction (SXRD) measurements were carried out at the I12-JEEP beamline [87] at the Diamond Light Source UK. As leather specimens were heated from ambient conditions to 250 °C and cooled down to 50 °C with a heating/cooling rate of 10 °C/min using a MFS350 Linkam stage, they were illuminated by an X-ray beam with an energy of 53.028 keV (corresponding to a wavelength of 0.23381 Å) and size of 0.5 × 0.5 mm^2. X-ray diffraction patterns were continuously collected in transmission mode by an area detector Pilatus 2 M CdTe detector [88]. The acquisition time per pattern was 30 s resulting in temperature resolution of 5 °C per pattern. 2D diffraction patterns were azimuthally integrated to obtain intensity curves using the DAWN software [89]. To simplify a comparison of the synchrotron data with laboratory data collected using a Cu anode, the synchrotron diffraction data were recalculated into 2θ space corresponding to a wavelength of a Cu Kα line (1.5406 Å).

The cytotoxicity tests were carried out as follow:

Cell cultures: Human keratinocytes HaCaT cells were grown in Dulbecco Modified Eagle's Medium with 10 % fetal bovine serum at 37 °C in a humidified atmosphere with 5 % CO_2. The cells were seeded at a cell density of 4 × 104 cells/ cm^2 in 96-well plates and left to adhere overnight. The samples were incubated with cells for 48 h.

MTT assay [90]: Cellular viability was measured using the 3-(4, 5-dimethylthiazol-2-yl)−2,5-diphenyltetrazolium bromide (MTT; Sigma-Aldrich, USA) assay. At the end of incubation period, the culture medium was removed, and the cells were incubated with 1 mg/mL MTT for 2 h at 37 °C. The purple formazan crystals formed in the viable cells were dissolved with 2-propanol (99 % purity, Sigma-Aldrich, USA) and the absorbance was measured at 595 nm using a plate multireader (GENios Tecan).

Lactate dehydrogenase (LDH) released [91] measurements were performed according to the following procedure: the culture medium was collected after 48 h of exposure, and LDH release was measured using Cytotoxicity Detection KitPLUS (Roche, USA) according to

manufacturer's instructions. Volumes of 50 μL culture supernatants were mixed with 50 μL Reaction mixture of catalyst and dye solution and incubated for 30 min in dark place. The absorbance was read at 490 nm using a microplate reader (Flex Station 3, Molecular Devices, USA).

The Antimicrobial Assay of composites on isolated microbes was performed by agar well diffusion method [92] according to EUCAST Guidelines, using MHA (Mueller Hinton Agar) plates [Screening of antibacterial potential of the prepared extracts against 1×10^5 CFU/mL *E. coli* (ATCC 11,229), 1×10^6 CFU/mL *Staphylococcus aureus* (ATCC 6538), 1×10^4 CFU/mL *Staphylococcus epidermis* (ATCC 12,228) and 1.5×10^5 CFU/mL *Brevibacterium* lines (ATCC 5274)].The total aerobic microbial count (TAMC) and total yeast and mould count (TYMC) assays were performed using Casein Soya Bean Digest Agar and Sabouraud Dextrose Agar. The plates were incubated at (30–35) °C for 1–2 days for TAMC and at (20–25) °C for 3–5 days for TYMC.

4. Conclusions

β-CD/HAp composites were obtained using the ultrasound-assisted technology. The use of ultrasound to reduce the size of the hydroxyapatite particles (sono-deagglomeration) proved effective, as did the use of cyclodextrin to confer the nano-HAp particles greater stability and solubility. The composites were chemically and structurally characterized by ATR-FTIR, TG/DTG, XRD and SEM analyses. The optimal parameters for the US treatment were determined based on the particle average size, zeta potential, polydispersity index and thermal degradation pattern. Treatment period is 30 min, with a 35 % amplitude and a β-CD:HAp ratio of 0.5:1. All of the composites exhibited antibacterial activity against *E. coli, S. aureus, B. linens* and *S. epidermidis*, and were non-cytotoxic. The interaction of composites with collagen from hide powder was proved by MHT method, micro-DSC and SEM. One composite was selected for the pilot scale test based on its particles' average dimension and stability in water suspension, thermal stability, char content and cost reasons. The leather specimen obtained by adding the ED8 composite in the re-tanning float demonstrated enhanced properties compared to the specimen obtained only with commercial products in terms of colour brightness, colour fastness, grain fullness, thickness, thermal stability, and breathability. All these enhanced performances of the leather treated with ED8 have been explained taking into account the specific properties of both β-CD and HAp. Interestingly, the thermal stability increase was proven at fiber and 3D-matrix levels (i.e., treated hide powder and treated leather in the re-tanning phase), while almost no bonds between collagen and ED8 are formed at the fibrillar level, which could have been detected by SXRD analysis. This may be due to the much larger size of the composite compared to the collagen fibrils. Considering all these findings and the green and safe procedures used to obtain the β-CD/HAp composites, as well as their lack of cytotoxicity and antibacterial activity, we cleared the way for a more sustainable leather processing without compromising the technical performance of the final product, but rather improving it. Other properties of the composite, such as flame retardancy, will be investigated and improved next.

Funding

This research was funded by a grant of the Ministry of Research, Innovation and Digitalization, CNCS/CCCDI UEFISCDI, Eureka project BIOSAFE LEATHER PN-III-P3–3.5-EUK-2019–0236 within PNCDI III. M. O., E.B, I.Q and C.P. acknowledge the funding for *in-situ* synchrotron-based X-ray diffraction measurements carried out at the I12-JEEP beamline at the Diamond Light Source UK (Experiment MG35634) offered by Diamond Light Source UK's National Synchrotron Science.

CRediT authorship contribution statement

Ilaria Quaratesi: Writing – original draft, Visualization, Project administration, Data curation, Conceptualization. **Ioan Călinescu:** Resources, Methodology, Conceptualization. **Petre Chipurici:** Resources, Investigation. **Elisa-Gabriela Dumbravă:** Visualization, Validation, Investigation, Formal analysis. **Andrei Cucos:** Validation, Resources, Data curation. **Mohamed Yassine Zaki:** Validation, Investigation, Data curation. **Pellegrino La Manna:** Writing – original draft, Visualization, Formal analysis. **Adrian Bercea:** Data curation. **Miruna Silvia Stan:** Investigation. **Stefan Michalik:** Software, Resources. **Chloe Pearce:** Software. **Marianne Odlyha:** Validation, Funding acquisition. **Genoveva Burca:** Software, Resources, Data curation. **Elena Badea:** Writing – review & editing, Supervision, Software, Resources, Project administration, Funding acquisition, Conceptualization.

Declaration of competing interest

The authors declare the following financial interests/personal relationships which may be considered as potential competing interests: Elena Badea reports financial support was provided by University of Craiova. Reports a relationship with that includes:. Has patent pending to. If there are other authors, they declare that they have no known competing financial interests or personal relationships that could have appeared to influence the work reported in this paper.

Acknowledgments

I.Q. acknowledge the receipt of the IULTCS Tyson Food Young Leather Scientist Grant 2023 for Basic Research; IQ is grateful for the Grant offered by Diamond Light source UK's National Synchrotron Science Facility to participate in the Experiment MG35634. The authors would like to thank Concepiò Casas and Anna Bacardit from the A3 Leather Innovation Centre, University of Lleida, for performing the pilot scale re-tanning test, and Rodica Roxana Constantinescu from INCDTP-ICPI for her assistance with the antimicrobial activity tests.

Supplementary materials

Supplementary material associated with this article can be found, in the online version, at doi:10.1016/j.molstruc.2024.141299.

Data availability

The raw data supporting the conclusions of this article will be made available by the authors on request.

References

[1] J. K, R.C. Panda, M. V.K, Trends and advancements in sustainable leather processing: future directions and challenges—A review, J. Environ. Chem. Eng. 8 (2020) 104379, https://doi.org/10.1016/j.jece.2020.104379.
[2] X. Chen, L. Xu, Z. Ren, F. Jia, Y. Yu, Sustainable supply chain management in the leather industry: a systematic literature review, Int. J. Logist. Res. Appl. 26 (2023) 1663–1703, https://doi.org/10.1080/13675567.2022.2104233.
[3] K. Fatema, Md.R. Sarker, K. Akhtar, A. Begum, S. Islam, Environmental sustainability: a challenge for leather industry, Leather Footwear J 23 (2023) 209–226, https://doi.org/10.24264/lfj.23.3.6.
[4] O. Omoloso, K. Mortimer, W.R. Wise, L. Jraisat, Sustainability research in the leather industry: a critical review of progress and opportunities for future research, J. Clean. Prod. 285 (2021) 125441, https://doi.org/10.1016/j.jclepro.2020.125441.
[5] S. Hueffer, T. Taeger, Sustainable leather manufacturing - A topic with growing importance 99 (2004) 424–428.
[6] F. Chiampo, S. Shanthakumar, R. Ricky, G.Pattukandan Ganapathy, Tannery: environmental impacts and sustainable technologies, Mater. Today Proc (2023), https://doi.org/10.1016/j.matpr.2023.02.025. S2214785323005436.
[7] J. Buljan, I. Kral, The framework for sustainable leather manufacture, Leather Work, Group LWG Milton Keynes UK (2019) 164.
[8] IULTCS, IUE 1 - recommendations on cleaner technologies for leather production, (2018). https://iultcs.org/wp-content/uploads/2020/07/All_IUE_documents.pdf.
[9] S.K. Rastogi, C. Kesavachandran, F. Mahdi, A. Pandey, Occupational cancers in leather tanning industries: a short review, Indian J Occup Env. Med 11 (2007) 3–5, https://doi.org/10.4103/0019-5278.32456.

[10] N.K. Chandra Babu, K. Asma, A. Raghupathi, R. Venba, R. Ramesh, S. Sadulla, Screening of leather auxiliaries for their role in toxic hexavalent chromium formation in leather—Posing potential health hazards to the users, J. Clean. Prod. 13 (2005) 1189–1195, https://doi.org/10.1016/j.jclepro.2004.07.003.
[11] D.D. Tegtmeyer, D.M. Kleban, Chromium and Leather Research (2014) 65.
[12] M. Dalamaga, D. Kounatidis, D. Tsilingiris, N.G. Vallianou, I. Karampela, S. Psallida, A.G. Papavassiliou, The role of endocrine disruptors bisphenols and phthalates in obesity: current evidence, perspectives and controversies, Int. J. Mol. Sci. (2024) 25, https://doi.org/10.3390/ijms25010675.
[13] C.R. China, M.M. Maguta, S.S. Nyandoro, A. Hilonga, S.V. Kanth, K.N. Njau, Alternative tanning technologies and their suitability in curbing environmental pollution from the leather industry: a comprehensive review, Chemosphere 254 (2020) 126804, https://doi.org/10.1016/j.chemosphere.2020.126804.
[14] S.S. Muthu, Leather and Footwear Sustainability, Springer, 2020.
[15] A. Haider, S. Haider, S.S. Han, I.-K. Kang, Recent advances in the synthesis, functionalization and biomedical applications of hydroxyapatite: a review, RSC. Adv. 7 (2017) 7442–7458, https://doi.org/10.1039/C6RA26124H.
[16] J. Beigbeder, J.-M. Lopez-Cuesta, Chapter 12 - Environmental challenges and perspectives in the development of nanocomposites for enhanced flame-retardant properties, in: S. Thomas, H. Vahabi, L. Somasekharan (Eds.), Flame Retard. Nanocomposites, Woodhead Publishing, 2024: pp. 369–424. 10.1016/B978-0-443-15421-8.00007-0.
[17] C. Ingrao, E. Vesce, R.S. Evola, E. Rebba, C. Arcidiacono, G. Martra, R. Beltramo, Chemistry behind leather: life Cycle Assessment of nano-hydroxyapatite preparation on the lab-scale for fireproofing applications, J. Clean. Prod. 279 (2021) 123837, https://doi.org/10.1016/j.jclepro.2020.123837.
[18] I. Quaratesi, M.C. Micu, E. Rebba, C. Carsote, N. Proietti, V. Di Tullio, R. Porcaro, E. Badea, Cleaner leather tanning and post-tanning processes using oxidized alginate as biodegradable tanning agent and nano-hydroxyapatite as potential flame retardant, Polymers. (Basel) 15 (2023) 4676, https://doi.org/10.3390/polym15244676.
[19] J. Zhu, X. Li, D. Li, C. Jiang, Thermal insulation and flame retardancy of the hydroxyapatite nanorods/sodium alginate composite aerogel with a double-crosslinked structure, ACS Appl. Mater. Interfaces 14 (2022) 45822–45831, https://doi.org/10.1021/acsami.2c12254.
[20] Chen Feng, Zhu Ying-Jie, Multifunctional calcium phosphate nanostructured materials and biomedical applications, Curr. Nanosci. 10 (2014) 465–485, https://doi.org/10.2174/1573413710666140319233658.
[21] U.G.K. Wegst, H. Bai, E. Saiz, A.P. Tomsia, R.O. Ritchie, Bioinspired structural materials, Nat. Mater 14 (2015) 23–36, https://doi.org/10.1038/nmat4089.
[22] M. Koizhaiganova, I. Yaşa, G. Gülümser, Assessment of antibacterial activity of lining leather treated with silver doped hydroxyapatite, Int. Biodeterior. Biodegrad. 105 (2015) 262–267, https://doi.org/10.1016/j.ibiod.2015.09.017.
[23] S. Selvaraju, S. Ramalingam, J.R. Rao, Preparation and application of biodegradable nanocomposite for cleaner leather processing, J. Clean. Prod. 158 (2017) 225–232, https://doi.org/10.1016/j.jclepro.2017.05.014.
[24] Y.Z. Wang, Z.H. Shan, The penetration and accumulation of hydroxyapatite and the hydrothermal stability of collagen matrix material, Mater. Chem. Phys. 226 (2019) 257–262, https://doi.org/10.1016/j.matchemphys.2019.01.030.
[25] K. Malisz, B. Świeczko-Żurek, J.-M. Olive, G. Gajowiec, G. Pecastaings, A. Laska, A. Sionkowska, Study of nanohydroxyapatite coatings prepared by the electrophoretic deposition method at various voltage and time parameters, Materials. (Basel) (2024) 17, https://doi.org/10.3390/ma17102242.
[26] K.R. Ramya, M. Sathish, B. Madhan, S.N. Jaisankar, P. Saravanan, Effective utilization of tannery hair waste to develop a high-performing re-tanning agent for cleaner leather manufacturing, J. Environ. Manage. 302 (2022) 114029, https://doi.org/10.1016/j.jenvman.2021.114029.
[27] N.N. Fathima, M.P. Kumar, J.R. Rao, B.U. Nair, A DSC investigation on the changes in pore structure of skin during leather processing, Thermochim. Acta 501 (2010) 98–102, https://doi.org/10.1016/j.tca.2010.01.016.
[28] L. Wang, X. Fan, Y. Sun, X. Sun, Effects of fibre pore status on hot-wet comfort of sheep garment leather, J. Soc. Leather Technol. Chem. 98 (2014) 113–120.
[29] V. Sivakumar, A. Jena, K. Gupta, A. Mandal, Analysis of Pore-size and related parameters for leather matrix through capillary flow porosimetry technique, J.-Soc. Leather Technol. Chem. 99 (2015) 16–22.
[30] C.A. Martínez-Pérez, J. García-Montelongo, P.E. Garcia Casillas, J.R. Farias-Mancilla, H. Monreal Romero, Preparation of hydroxyapatite nanoparticles facilitated by the presence of β-cyclodextrin, Int. Symp. Metast. Amorph. Nanostruct. Mater 536 (2012) S432–S436, https://doi.org/10.1016/j.jallcom.2011.12.135. ISMANAM-2011 26th June July 1st 2011.
[31] K.D. Son, Y.-J. Kim, Morphological structure and characteristics of hydroxyapatite/β-cyclodextrin composite nanoparticles synthesized at different conditions, Mater. Sci. Eng. C 33 (2013) 499–506, https://doi.org/10.1016/j.msec.2012.09.020.
[32] T. Wimmer, in Cyclodextrins, Ullmanns Encycl. Ind. Chem. (2003), https://doi.org/10.1002/14356007.e08_e02.
[33] E.M.M. Del Valle, Cyclodextrins and their uses: a review, Process. Biochem. 39 (2004) 1033–1046, https://doi.org/10.1016/S0032-9592(03)00258-9.
[34] X. Li, L. Xie, X. Yang, X. Nie, Adsorption behavior and mechanism of β-cyclodextrin–styrene-based polymer for cationic dyes, RSC. Adv. 8 (2018) 40321–40329, https://doi.org/10.1039/C8RA07709F.
[35] X. Liu, X. Zhang, W. Chen, C.C. Gaidau, L. Miu, Preparation of a Colored B-cyclodextrin fragrance agent for leather finishing, Leather Footwear J 13 (2013) 139–148, https://doi.org/10.24264/lfj.13.2.4.
[36] R. Periasamy, A systematic review on the significant roles of cyclodextrins in the construction of supramolecular systems and their potential usage in various fields, J. Carbohydr. Chem. 39 (2020) 189–216, https://doi.org/10.1080/07328303.2020.1792919.
[37] X. Dang, H. Qiu, S. Qu, S. Liang, L. Feng, X. Wang, β-Cyclodextrin-based chrome-free tanning agent results in the sustainable and cleaner production of eco-leather, ACS Sustain. Chem. Eng. 12 (2024) 3715–3725, https://doi.org/10.1021/acssuschemeng.3c07446.
[38] I. Quaratesi, I. Bruno, A. Pauciulo, A.R. Bartiromo, E. Badea, C. Carşote, P. Neri, C. Talotta, R. Gliubizzi, V. Di Tullio, N. Proietti, A. Cepparrone, F. Nuti, V. Ferrara, C. Gaeta, Side-chain Poly[2]pseudorotaxanes containing β-cyclodextrin for more sustainable tanning process, Polym. Test. 129 (2023) 108268, https://doi.org/10.1016/j.polymertesting.2023.108268.
[39] S. Liang, X. Wang, S. Sun, D. Hao, L. Xie, J. Yang, X. Dang, Polysaccharides for sustainable leather production: a review, Environ. Chem. Lett. 22 (2024) 2553–2572, https://doi.org/10.1007/s10311-024-01744-0.
[40] G. Abdel-Maksoud, H.E.-S. Nasr, S.H. Samaha, M.S.-El. Kassem, Evaluation of the performance of Hydroxypropyl-β-cyclodextrin for the consolidation of vegetable-tanned leather artifacts, Herit. Sci. 12 (2024) 188, https://doi.org/10.1186/s40494-024-01294-2.
[41] Gowri, Venkatesan, Anil, Sudha, Physico-chemical characterization and antimicrobial efficiency of beta-cyclodextrin/hydroxyapatite composite, (2019). 10.5281/zenodo.5652765.
[42] G. Gowri, P.N. S, Synthesis and characterisation of β-cyclodextrin and hydroxyapatite composite by ultrasonication method, World J. Pharm. Res. 7 (2018) 1242–1249, https://doi.org/10.20959/wjpr20184-11163.
[43] V. Sivakumar, P.G. Rao, Sonochemical applications for process industries: a comprehensive analysis and review, Trans. Indian Natl. Acad. Eng. 9 (2024) 1–24, https://doi.org/10.1007/s41403-023-00444-5.
[44] M. Kamali, R. Dewil, L. Appels, T.M. Aminabhavi, Nanostructured materials via green sonochemical routes – Sustainability aspects, Chemosphere 276 (2021) 130146, https://doi.org/10.1016/j.chemosphere.2021.130146.
[45] A. Rosales Pérez, K.Esquivel Escalante, The evolution of sonochemistry: from the beginnings to novel applications, Chempluschem. 89 (2024) e202300660, https://doi.org/10.1002/cplu.202300660.
[46] G. Chatel, How sonochemistry contributes to green chemistry?, SI ESS-15 2016 Istanb. 40 (2018) 117–122. doi:10.1016/j.ultsonch.2017.03.029.
[47] A. Rosales Pérez, K.Esquivel Escalante, The evolution of sonochemistry: from the beginnings to novel applications, Chempluschem. 89 (2024) e202300660, https://doi.org/10.1002/cplu.202300660.
[48] M.D. Luque de Castro, F. Priego-Capote, Ultrasound-assisted crystallization (sonocrystallization), Ultrason. Sonochem. 14 (2007) 717–724, https://doi.org/10.1016/j.ultsonch.2006.12.004.
[49] H.N. Kim, K.S. Suslick, The effects of ultrasound on crystals: sonocrystallization and sonofragmentation, Crystals 8 (2018), https://doi.org/10.3390/cryst8070280.
[50] M. Sathish, B. Madhan, J.Raghava Rao, Leather solid waste: an eco-benign raw material for leather chemical preparation – A circular economy example, Waste Manage 87 (2019) 357–367, https://doi.org/10.1016/j.wasman.2019.02.026.
[51] A. Doostmohammadi, A. Monshi, R. Salehi, M.H. Fathi, Z. Golniya, Alma. U. Daniels, Bioactive glass nanoparticles with negative zeta potential, Ceram. Int 37 (2011) 2311–2316, https://doi.org/10.1016/j.ceramint.2011.03.026.
[52] Zeta Potential Measurement J.D. Clogston, A.K. Patri, in: S.E. McNeil (Ed.), Charact. Nanoparticles Intend. Drug Deliv. (2011) 63–70, https://doi.org/10.1007/978-1-60327-198-1_6.
[53] S. Nalesso, M.J. Bussemaker, R.P. Sear, M. Hodnett, J. Lee, A review on possible mechanisms of sonocrystallisation in solution, Ultrason. Sonochem. 57 (2019) 125–138, https://doi.org/10.1016/j.ultsonch.2019.04.020.
[54] G. Roebben, S. Ramirez-Garcia, V.A. Hackley, M. Roesslein, F. Klaessig, V. Kestens, I. Lynch, C.M. Garner, A. Rawle, A. Elder, V.L. Colvin, W. Kreyling, H.F. Krug, Z. A. Lewicka, S. McNeil, A. Nel, A. Patri, P. Wick, M. Wiesner, T. Xia, G. Oberdörster, K.A. Dawson, Interlaboratory comparison of size and surface charge measurements on nanoparticles prior to biological impact assessment, J. Nanoparticle Res. 13 (2011) 2675–2687, https://doi.org/10.1007/s11051-011-0423-y.
[55] A. Antonakos, E. Liarokapis, T. Leventouri, Micro-Raman and FTIR studies of synthetic and natural apatites, Biomaterials 28 (2007) 3043–3054, https://doi.org/10.1016/j.biomaterials.2007.02.028.
[56] O. Egyed, Spectroscopic studies on β-cyclodextrin, Vib. Spectrosc. 1 (1990) 225–227, https://doi.org/10.1016/0924-2031(90)80041-2.
[57] A. Bergal, M. Andac, Fabrication and Investigation of Oxidized-β-Cyclodextrin Nanoparticle as a Novel Class pH Responsive Drug Delivery Vehicle, J. Polym. Environ. (2023), https://doi.org/10.1007/s10924-023-03082-8.
[58] B. Viswanath, N. Ravishankar, Controlled synthesis of plate-shaped hydroxyapatite and implications for the morphology of the apatite phase in bone, Biomaterials 29 (2008) 4855–4863, https://doi.org/10.1016/j.biomaterials.2008.09.001.
[59] D. Haojie, J. Liuyun, M. Bingli, S. Shengpei, T. Shuo, T. Chunyan, W. Jinghui, L. Zhiwei, H. Xiang, Synthesis of a novel co-hybridization nano-apatite powder with excellent dispersion, well-solubility and good biocompatibility by a new strategy, Adv. Powder Technol. 30 (2019) 485–492, https://doi.org/10.1016/j.apt.2018.11.026.
[60] I. Shown, S. Banerjee, A.V. Ramchandran, K.E. Geckeler, C.N. Murthy, Synthesis of cyclodextrin and sugar-based oligomers for the efavirenz drug delivery, Macromol. Symp. 287 (2010) 51–59, https://doi.org/10.1002/masy.201050108.
[61] F. Trotta, M. Zanetti, G. Camino, Thermal degradation of cyclodextrins, Polym. Degrad. Stab. 69 (2000) 373–379, https://doi.org/10.1016/S0141-3910(00)00084-7.
[62] M.S. Djošić, V.B. Mišković-Stanković, S. Milonjić, Z.M. Kačarević-Popović, N. Bibić, J. Stojanović, Electrochemical synthesis and characterization of hydroxyapatite

powders, Mater. Chem. Phys. 111 (2008) 137–142, https://doi.org/10.1016/j.matchemphys.2008.03.045.
[63] S. Vijayan, T. Merlin, M.S. Jisha, Chapter 11 - Biocompatibility and cytotoxicity of polymer sutures, in: S. Thomas, P. Coates, B. Whiteside, B. Joseph, K. Nair (Eds.), Chapter 11 - Biocompatibility and cytotoxicity of polymer sutures, Adv. Technol. Polym. Mater. Surg. Sutures (2023) 249–264, https://doi.org/10.1016/B978-0-12-819750-9.00009-7.
[64] S. Lamkhao, M. Phaya, C. Jansakun, N. Chandet, K. Thongkorn, G. Rujijanagul, P. Bangrak, C. Randorn, Synthesis of hydroxyapatite with antibacterial properties using a microwave-assisted combustion method, Sci. Rep. 9 (2019) 4015, https://doi.org/10.1038/s41598-019-40488-8.
[65] G.S. Kumar, S. Rajendran, S. Karthi, R. Govindan, E.K. Girija, G. Karunakaran, D. Kuznetsov, Green synthesis and antibacterial activity of hydroxyapatite nanorods for orthopedic applications, MRS. Commun. 7 (2017) 183–188, https://doi.org/10.1557/mrc.2017.18.
[66] E. Badea, C. Şendrea, C. Carşote, A. Adams, B. Blümich, H. Iovu, Unilateral NMR and thermal microscopy studies of vegetable tanned leather exposed to dehydrothermal treatment and light irradiation, Microchem. J. 129 (2016) 158–165, https://doi.org/10.1016/j.microc.2016.06.013.
[67] C. Carsote, E. Badea, Micro differential scanning calorimetry and micro hot table method for quantifying deterioration of historical leather, Herit. Sci. 7 (2019) 48, https://doi.org/10.1186/s40494-019-0292-8.
[68] E. Badea, G. Della Gatta, T. Usacheva, Effects of temperature and relative humidity on fibrillar collagen in parchment: a micro differential scanning calorimetry (micro DSC) study, Polym. Degrad. Stab. 97 (2012) 346–353, https://doi.org/10.1016/j.polymdegradstab.2011.12.013.
[69] C.A. Miles, M. Ghelashvili, Polymer-in-a-box mechanism for the thermal stabilization of collagen molecules in fibers, Biophys. J. 76 (1999) 3243–3252.
[70] F.M. Bezerra, M.J. Lis, H.B. Firmino, J.G. Dias Da Silva, R.D.C.S. Curto Valle, J. A. Borges Valle, F.A.P. Scacchetti, A.L. Tessaro, The Role of β-Cyclodextrin in the Textile Industry—Review, Molecules. 25 (2020) 3624, https://doi.org/10.3390/molecules25163624.
[71] S. Pereva, V. Nikolova, S. Angelova, T. Spassov, T. Dudev, Water inside β-cyclodextrin cavity: amount, stability and mechanism of binding, Beilstein J. Org. Chem. 15 (2019) 1592–1600, https://doi.org/10.3762/bjoc.15.163.
[72] X. Wang, H. Wu, X. Cheng, M. Yang, L. Zhang, Probing the surface activity of hydroxyapatite nanoparticles through their interaction with water molecules, AIP. Adv. 10 (2020) 065217, https://doi.org/10.1063/5.0010750.
[73] A. Adams, Non-destructive analysis of polymers and polymer-based materials by compact NMR, Magn. Reson. Imaging 56 (2019) 119–125, https://doi.org/10.1016/j.mri.2018.09.015.
[74] D. Capitani, V. Di Tullio, N. Proietti, Nuclear magnetic resonance to characterize and monitor cultural heritage, Prog. Nucl. Magn. Reson. Spectrosc. 64 (2012) 29–69, https://doi.org/10.1016/j.pnmrs.2011.11.001.
[75] C. Sendrea, C. Carsote, M. Radu, E. Badea, L. Miu, The effect of gamma irradiation on shrinkage activity of collagen in vegetable tanned leather, Rev Chim 68 (2017) 1535–1538.
[76] N.N. Fathima, M. Baias, B. Blumich, T. Ramasami, Structure and dynamics of water in native and tanned collagen fibers: effect of crosslinking, Int. J. Biol. Macromol. 47 (2010) 590–596, https://doi.org/10.1016/j.ijbiomac.2010.08.003.
[77] C. Carsote, C. Şendrea, M.-C. Micu, A. Adams, E. Badea, Micro-DSC, FTIR-ATR and NMR MOUSE study of the dose-dependent effects of gamma irradiation on vegetable-tanned leather: the influence of leather thermal stability, Radiat. Phys. Chem. 189 (2021) 109712, https://doi.org/10.1016/j.radphyschem.2021.109712.
[78] I. Quaratesi, M.C. Micu, E. Rebba, C. Carsote, N. Proietti, V. Di Tullio, R. Porcaro, E. Badea, Cleaner leather tanning and post-tanning processes using oxidized alginate as biodegradable tanning agent and nano-hydroxyapatite as potential flame retardant, Polymers 15 (2023) 4676. doi:10.3390/polym15244676.
[79] E. Bañón, A.N. García, A. Marcilla, Thermogravimetric analysis and Py-GC/MS for discrimination of leather from different animal species and tanning processes, J. Anal. Appl. Pyrolysis 159 (2021) 105244, https://doi.org/10.1016/j.jaap.2021.105244.
[80] G.Sanchez Olivares, A. Battig, S.M. Goller, D. Rockel, V.R. González, B. Schartel, Imparting Fire Retardancy and Smoke Suppression to Leather during Tanning Processes, ACS. Omega 7 (2022) 44156–44169, https://doi.org/10.1021/acsomega.2c05633.
[81] T.A. Grünewald, M. Liebi, H. Birkedal, Crossing length scales: x-ray approaches to studying the structure of biological materials, IUCrJ. 11 (2024) 708–722, https://doi.org/10.1107/S2052252524007838.
[82] C.A. Maxwell, T.J. Wess, C.J. Kennedy, X-ray diffraction study into the effects of liming on the structure of collagen, Biomacromolecules. 7 (2006) 2321–2326, https://doi.org/10.1021/bm060250t.
[83] E. Badea, T.R. Usacheva, G.Della Gatta, The use of differential scanning calorimetry to characterise collagen deterioration in parchment, Российский ХиМический Журнал 59 (2015) 28–41.
[84] R. Naffa, C. Maidment, M. Ahn, B. Ingham, S. Hinkley, G. Norris, Molecular and structural insights into skin collagen reveals several factors that influence its architecture, Int. J. Biol. Macromol. 128 (2019) 509–520, https://doi.org/10.1016/j.ijbiomac.2019.01.151.
[85] F. Cappa, I. Paganoni, C. Carsote, M. Schreiner, E. Badea, Studies on the effect of dry-heat ageing on parchment deterioration by vibrational spectroscopy and micro hot table method, Polym. Degrad. Stab. 182 (2020) 109375, https://doi.org/10.1016/j.polymdegradstab.2020.109375.
[86] P. Narayanan, S.K. Janardhanan, An approach towards identification of leather from leather-like polymeric material using FTIR-ATR technique, Collagen Leather 6 (2024) 1, https://doi.org/10.1186/s42825-023-00145-3.
[87] M. Drakopoulos, T. Connolley, C. Reinhard, R. Atwood, O. Magdysyuk, N. Vo, M. Hart, L. Connor, B. Humphreys, G. Howell, S. Davies, T. Hill, G. Wilkin, U. Pedersen, A. Foster, N. De Maio, M. Basham, F. Yuan, K. Wanelik, I12: the joint engineering, environment and processing (jeep) beamline at diamond light source, J. Synchrotron Radiat 22 (2015) 828–838, https://doi.org/10.1107/S1600577515003513.
[88] D. Šišak Jung, T. Donath, O. Magdysyuk, J. Bednarcik, High-energy X-ray applications: current status and new opportunities, Powder. Diffr. 32 (2017) S22–S27, https://doi.org/10.1017/S0885715617001191.
[89] J. Filik, A.W. Ashton, P.C.Y. Chang, P.A. Chater, S.J. Day, M. Drakopoulos, M. W. Gerring, M.L. Hart, O.V. Magdysyuk, S. Michalik, A. Smith, C.C. Tang, N. J. Terrill, M.T. Wharmby, H. Wilhelm, Processing two-dimensional X-ray diffraction and small-angle scattering data in *DAWN 2*, J. Appl. Crystallogr. 50 (2017) 959–966, https://doi.org/10.1107/S1600576717004708.
[90] J.C. Stockert, R.W. Horobin, L.L. Colombo, A. Blázquez-Castro, Tetrazolium salts and formazan products in Cell Biology: viability assessment, fluorescence imaging, and labeling perspectives, Acta Histochem. 120 (2018) 159–167, https://doi.org/10.1016/j.acthis.2018.02.005.
[91] P. Kumar, A. Nagarajan, P.D. Uchil, Analysis of cell viability by the lactate dehydrogenase assay, Cold Spring Harb. Protoc. (2018), 2018pdb.prot095497.
[92] European directorate for the quality of medicines & healthcare, European Pharmacopeia 10th Edition continuous upgrade to address new challenges-September 2019, (2019). https://www.edqm.eu/en/d/85150 (accessed March 20, 2024).